Chemical Geology 391 (2015) 56–73

Contents lists available at ScienceDirect

Chemical Geology

journal homepage: www.elsevier.com/locate/chemgeo

Toward a quantitative model for the formation of gravitational magmatic sulfide deposits

Youxue Zhang *

Department of Earth & Environmental Sciences, The University of Michigan, Ann Arbor, MI 48109-1005, USA

ARTICLE INFO

Article history:
Received 19 April 2014
Received in revised form 25 October 2014
Accepted 28 October 2014
Available online 3 November 2014

Editor: L. Reisberg

Keywords:
Magmatic sulfide ores
Kinetics
Dynamics
Diffusive fractionation
Gravitational settling

ABSTRACT

A preliminary quantitative model for the formation of magmatic sulfide deposits through gravitational sulfide droplet settling is developed. The model incorporates thermodynamic consideration of the oversaturation of sulfide liquid from a silicate melt, and the coupled growth kinetics and settling dynamics of sulfide droplets. The conditions for the sulfide droplets to have enough time to grow and settle to form a sulfide liquid layer at the bottom of a magma chamber are referred to as the necessary criteria for sulfide ore formation. Simulations are carried out for dry Etna basaltic melt because their melt viscosity and sulfur diffusivity have been measured so that the simulations are more realistic rather than parametric. Furthermore, the effects of empirical nucleation rate and condition, and of the variation of solubility, viscosity and diffusivity have been parametrically evaluated. The simulations show that for a given magma containing about 0.1 to 0.3 wt.% sulfur, sulfide melt layer can form for realistic magma body size (with cooling time of 1000 yr or more) and realistic solubility, viscosity and diffusivity. The ability of the sulfide melt to collect ore elements depends critically on the diffusivity of individual ore elements. When the diffusivity of an ore element is similar to or greater than that of sulfur, near equilibrium partitioning is reached. When the diffusivity of an ore element is much smaller than that of sulfur, which is often the case for trivalent and tetravalent ions, the concentration of the element in the sulfide melt would be far below the equilibrium concentration. It is hoped that the model will help both researchers and exploration geologists.

1. Introduction

Magmatic sulfide deposits of Ni–Cu–PGE are critical resources for industrial development. About 60% of the world's Ni and 40% of the world's PGE (platinum-group elements) are mined from magmatic sulfide deposits (Bremond d'Ars et al., 2001). With the rise of many developing nations, the world's need for metal deposits increased rapidly in recent years, and the mining industry is booming and becoming increasingly more important. This work focuses on magmatic sulfide deposits, and does not cover hydrothermal sulfide deposits and porphyry-type deposits.

Magmatic sulfide deposits form by the oversaturation and separation of sulfide liquid from silicate liquid (two-liquid immiscibility), as sketched in Fig. 1 (Naldrett, 1989; Bremond d'Ars et al., 2001; Mungall and Naldrett, 2008). A mafic silicate melt typically contains a significant amount of sulfur (e.g., 0.10–0.25 wt.%, Wallace and Carmichael, 1992). As the melt cools, the sulfur concentration at sulfide saturation (referred to as sulfur solubility for simplicity) decreases. As the melt fractionates silicate and oxide phases, the concentration of sulfur increases. Assimilation of country rocks or magma mixing may also cause sulfide saturation (Simon and Ripley, 2011; Ripley and Li, 2013). At some point, sulfide liquid becomes supersaturated (e.g., at a temperature of about 1510 K when S concentration in a basaltic melt is 0.16 wt.% using the solubility model of Li and Ripley, 2009), and sulfide melt (composition not too different from FeS) forms due to immiscibility between sulfide and silicate liquids. The nucleation and growth of sulfide liquid droplets may be kinetically hindered. The droplets sink through silicate melt due to higher density of the sulfide melt, and accumulate at the bottom of the magma body, often with other crystallizing and dense minerals such as olivine, pyroxene and chromite. Depending on how completely sulfide melts segregated from silicate minerals, one may observe massive sulfide, or semi-massive net-textured sulfide, or disseminated sulfide ores (Simon and Ripley, 2011). The formation of a sulfide deposit requires both the segregation of the sulfide liquid and the concentration of ore elements in the sulfide liquid. The critical processes for magmatic sulfide deposit formation in this mechanism include the formation, growth and settling of sulfide droplets through a sufficient distance, and accumulation at the bottom of a magma body. Otherwise, either sulfur is dispersed in various minerals or sulfide droplets are dispersed in the rock without forming a layer with high concentration of sulfide, meaning no economic value. It is therefore necessary to understand the equilibrium between sulfide melt and silicate melt, as well as the nucleation and growth kinetics and settling dynamics of

* Tel.: +1 734 763 0947.
E-mail address: youxue@umich.edu.

http://dx.doi.org/10.1016/j.chemgeo.2014.10.025
0009-2541/

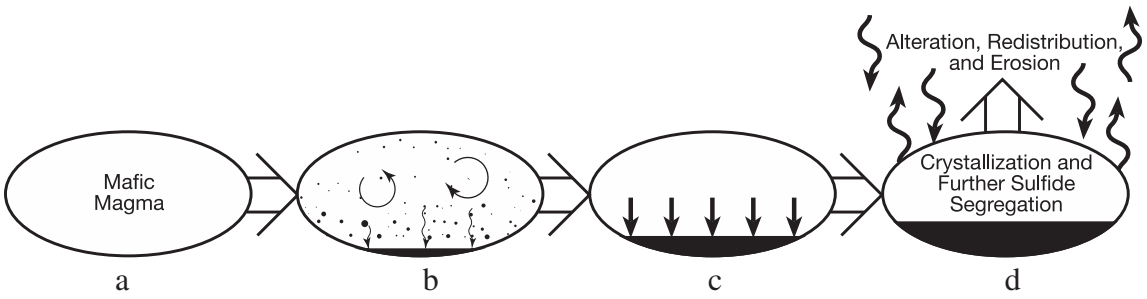

Fig. 1. Processes for magmatic sulfide deposit formation.
Adapted from Naldrett, 1989.

droplets in order to quantitatively model the formation of such deposits. In addition, it is critical to assess the conditions for the sulfide liquid to scavenge Ni–Cu–PGE elements (e.g., Mungall, 2002a). Other important considerations include the role of olivine fractionation (e.g., Simon and Ripley, 2011; Ripley and Li, 2013), and the role of conduit systems (e.g., Chai and Naldrett, 1992; Li et al., 2000; Maier et al., 2001; Ding et al., 2010) in sulfide ore formation.

The equilibrium thermodynamics of sulfide formation in silicate melts have been investigated for about 60 yr and it is now possible to predict sulfur concentration at sulfide saturation (e.g., Fincham and Richardson, 1954; Naldrett, 1969; Li and Ripley, 2009; Baker and Moretti, 2011, and references therein). On the other hand, the kinetics and dynamics of magmatic sulfide ore formation have not been explored much in the literature (but see Mungall, 2002a; Holzheid, 2010), and is the focus of this work. It is not known to what degree the formation, growth and gravitational settling of sulfide droplets are kinetically and dynamically controlled. The *kinetics* involves the nucleation and growth of the droplet, which requires the transport (diffusion and convection) of S (and Fe and ore elements) from the silicate melt into the sulfide melt. Because S concentration in silicate melt is low, a large volume of silicate melt must be depleted to grow a sulfide droplet. For example, if the saturation concentration is 0.11 wt.% and the bulk S concentration in the silicate melt is 0.12 wt.%, to grow a small sulfide droplet (~36 wt.% S) of 1 mm diameter, a sphere of silicate melt with a diameter of ≥17 mm must be depleted and the mean growth time would be about 4 yr assuming pure diffusion transport at the saturation temperature. For a cooling melt, equilibrium may never be reached. Another consequence of low sulfide concentration is that on average sulfide droplets are far separated from one another, meaning that coalescence is not important except when the droplets reach the bottom accumulating layer.

The *dynamics* involves the gravitational settling of sulfide droplets through silicate melt to the bottom of the magma body due to higher density of sulfide melt, essential for sulfide melt to accumulate at the bottom of a magma body to form sulfide deposits, without which sulfide would be dispersed in the igneous rock with no economic value. Furthermore, there is positive feedback between growth and settling: e.g., larger drops sink more rapidly, and more rapid settling enhances mass transfer and growth.

Whether a sulfide deposit contains enough ore elements depends on (i) the initial content of the ore-forming elements in the magma, (ii) the partitioning of the ore elements between sulfide and silicate melts, and (iii) whether the diffusivity is high for them to diffuse into sulfide droplets. The first can be evaluated by inferring the primary melt composition (e.g., from melt inclusion studies), the second can be determined by measuring the partition coefficients (e.g., Peach et al., 1990; Kiseeva and Wood, 2013) and developing elemental distribution models (Shaw, 1970), and the third can be assessed by comparing the diffusivity of the ore-forming elements (largely unknown) with that of sulfur and by modeling diffusion of these elements into the droplets once the growth and settling of sulfide droplets are quantified. Boudreau and Meurer (1999) explored the chromatographic separation of ore elements and sulfur during degassing and solidification, and Mungall (2002a) modeled some aspects of kinetics controls on the partitioning of ore elements between sulfide and silicate liquids at constant temperature.

Based on the above consideration, the most important controls for magmatic sulfide layer formation are: high initial sulfur concentration and relatively slow cooling so that there is enough time for the sulfide droplet to form and settle. For the sulfide layer to be an ore deposit, the initial Ni–Cu–PGE concentrations must be high enough and these elements must be able to be collected by sulfide melt. This work presents a preliminarily model for the processes of sulfide melt nucleation, growth, settling and accumulation, as well as the collection of ore elements during sulfide drop growth and settling, as a step toward a quantitative and predictive model for the formation of magmatic sulfide deposits by gravitational settling. It is hoped that the model will gradually evolve to become accurate enough in understanding sulfide ore formation so as to be a practical and predictive tool in sulfide ore exploration.

There is a large literature on liquid metal settling in a silicate magma ocean during core formation (e.g., Rubie et al., 2003, 2011; Ziethe, 2009; Ichikawa et al., 2010; Deguen et al., 2011). These models treat mass transfer between a falling metal droplet and the surrounding silicate melt, but do not consider droplet growth or dissolution during sinking. Ignoring growth kinetics is probably OK in these models because Fe concentration in the magma ocean was high during core formation, meaning iron drop size is probably not much controlled by mass transfer but more controlled by drop stability. However, during sulfide droplet growth and settling, S concentration is low and kinetics are important in controlling droplet size. Also due to high Fe concentration in a magma ocean and low S concentration in a magma chamber, coalescence is important during core formation (Ichikawa et al., 2010), but unimportant during sulfide deposit formation except when sulfide drops are concentrated near the bottom. Hence, the core formation models cannot be applied to model sulfide deposit formation.

2. Model

The formation of sulfide ore deposits in the context of gravitational settling is controlled by not only thermodynamics (sulfide melt supersaturation), but also kinetics (sulfide droplet growth) and dynamics (sulfide droplet settling). Hence, a quantitative model must consider all of these aspects. The *thermodynamics* includes the saturation of sulfide melt. The *kinetics* involves the nucleation and growth of sulfide droplets, and the growth requires the transport (diffusion and convection) of S and ore elements from the silicate melt into the sulfide melt. For a cooling melt, equilibrium may not be reached and hence it is necessary to quantify the kinetics. The *dynamics* involves the gravitational settling of sulfide droplets through silicate melt to the bottom of the magma body, essential for sulfide melt to accumulate at the bottom of a magma body to form sulfide deposits, without which sulfide would

be dispersed in the igneous rock. There is positive feedback between growth and settling: larger drops sink more rapidly, and more rapid settling enhances mass transfer and growth. In sulfide deposit literature, thermodynamic aspects and the factors affecting S concentration and solubility in the melt such as fractionation, assimilation and magma mixing, were carefully considered (e.g., Naldrett, 1989, 2004; Mungall and Naldrett, 2008; Ripley and Li, 2013), but kinetic and dynamic aspects have not been explored much. This work adds consideration of the kinetic and dynamic controls in addition to thermodynamic controls. Below, some basic aspects are elucidated first, and detailed modeling steps are explained subsequently.

A silicate melt at high temperature with some initial S concentration undergoes cooling, with simultaneous fractionation, and possibly assimilation and magma mixing. Sulfide saturation temperature can be calculated from a recent solubility model for sulfide sulfur (meaning sulfur in the form of sulfide, not sulfate; hereafter sulfur means sulfide sulfur unless otherwise noted) (e.g., Li and Ripley, 2005; Moretti and Otonnello, 2005; Liu et al., 2007; Kress et al., 2008; Moretti and Baker, 2008; Jugo, 2009; Li and Ripley, 2009; Baker and Moretti, 2011). With supersaturation, sulfide droplets nucleate in the silicate melt (Fig. 1b). The nucleation rate depends on the degree of supersaturation and the surface tension, among other factors. Unfortunately, it is not possible yet to calculate nucleation rate as a function of temperature and sulfur concentration because sulfide droplet nucleation rates have not been experimentally determined and the classical nucleation theory is not adequate (Zhang, 2008, Section 4.1.1) unless the surface tension as a function of temperature is obtained by fitting experimental nucleation data. For example, using the interface energy between sulfide and silicate liquids determined by Mungall and Su (2005), the classical nucleation theory would require more than 1.1 wt.% S to have a noticeable homogeneous nucleation rate (1 m^{-3} yr^{-1}), and heterogeneous nucleation on silicate minerals is not an option either (Mungall and Su, 2005). However, natural mid-ocean ridge basaltic glasses containing 0.1–0.2 wt.% S often contain sulfide globules (Wallace and Carmichael, 1992; Patten et al., 2013), indicating that nucleation does occur, contrary to the prediction of classical nucleation theory. To circumvent this difficulty, nucleation of sulfide melt droplets is treated by assuming that it occurs at some fixed degree of supersaturation. As such, the nucleation temperature can be calculated from a solubility model, and the starting droplet radius can be calculated as the critical radius (a droplet at this radius is at the Gibbs free energy maximum and adding more FeS molecules to it will decrease its Gibbs free energy and cause it to grow stably). Upon further cooling, sulfide droplets grow and sink (Figs. 1b and 2). The growth is controlled by mass transfer of sulfur involving both diffusion and convection (Zhang et al., 1989; Kerr, 1995; Zhang and Xu, 2003). The composition of the sulfide droplet is typically close to FeS (Naldrett, 1989) with minor amounts of other elements, especially the important ore elements including Cu, Ni, PGE, and others. Although both Fe and S are major elements in the sulfide melt, due to the low concentration of S in a basaltic melt (typically 0.18 wt.%) and high concentration of Fe in a basaltic melt (typically 10 wt.%), it is necessary for S to travel through a large distance to supply nutrient for sulfide droplet growth. That is, S is the principal equilibrium determining component (Zhang et al., 1989) and S diffusion rather than Fe diffusion limits the growth rate of sulfide droplets. Because sulfide melt is denser than silicate melt, the sulfide droplets will sink in silicate melt. The falling of a sulfide droplet induces convection around it (e.g., removing the silicate liquid on the leading or lower side of the droplet), and the growth of sulfide droplets is not purely diffusive (Zhang et al., 1989; Chen and Zhang, 2008, 2009), but is convective (Kerr, 1995), meaning that mass transfer is accomplished by not only diffusion but also enhanced by convection. Theory for convective growth rate has been developed by Kerr (1995) and Zhang and Xu (2003) (see also review by Zhang, 2013). By simultaneously calculating the convective growth rate and falling velocity at each time step, the growth and descent can be quantified, as applied successfully to halide crystal dissolution in aqueous solutions (Kerr, 1995; Zhang and Xu, 2003), CO_2 drop dissolution in seawater (Zhang, 2005) and bubble growth in beer (Zhang and Xu, 2008). For the sulfide deposit formation, the falling distance must be about the thickness of the magma body, so that a bottom sulfide layer can form, a pre-requisite for magmatic sulfide deposits. The detailed modeling steps and assumptions are as follows.

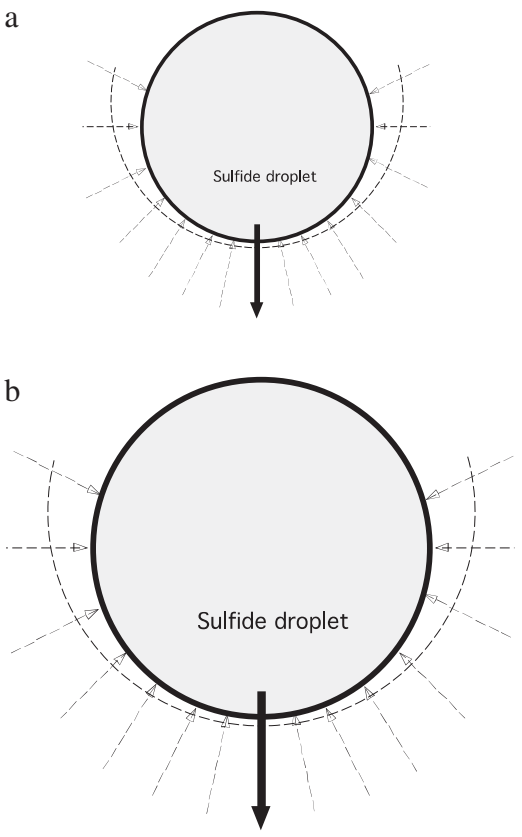

Fig. 2. The growth and sinking of a sulfide droplet in a silicate melt. In each panel, the circle represents a spherical sulfide droplet, and the region between the circle and dashed curve represents the compositional boundary layer (silicate melt). The heavy solid arrow indicates the falling direction, and the thin dashed arrows indicate mass transfer into the droplet. As it falls from a to b, the droplet grows. The detailed model for the growth of a sinking sphere has been developed by Kerr (1995) and Zhang and Xu (2003) and briefly outlined here in Eqs. (5)–(10).

1. In this work, a generic single stage exponential cooling history (Zhang, 1994, 2008) for the magma chamber is assumed:

$$T = T_\infty + (T_0 - T_\infty)\exp(-t/\tau), \quad (1)$$

where T_∞ is the ambient temperature (assumed to be 300 K hereafter, though it may also be the country rock temperature higher than 300 K), T_0 is the initial temperature (taken as the temperature at which nucleation occurs), and τ is the cooling time scale (e.g., 10,000 yr) and can be varied (all the symbols are explained in Table 1.). If the cooling history has been modeled for the given magma body by considering heat conduction and convection, that temperature as a function of time and position in the magma chamber can be used without free parameters.
2. Crystal fractionation of the magma body provides important controls in sulfide deposit formation. Crystal fractionation produces at least the following effects:
   (i) The melt composition will vary, including sulfur concentration increase and major oxide composition variation. The former leads to easier formation of sulfide droplets, and the latter will change sulfur solubility (most likely decrease), melt viscosity (most likely increase) and density (most likely decrease), and

Table 1
Symbols.

a	Radius of sulfide droplet
a_0	Initial radius of sulfide droplet, taken to be the radius of the critical nuclei
C	Concentration in the melt. If not otherwise stated, it is sulfur concentration in wt.%
C_0	Initial sulfur concentration in the silicate melt
C_∞	Sulfur concentration in the far-field silicate melt (decreases as sulfide liquid volume grows)
$C\|_{r=a}$	Sulfur concentration at the interface silicate melt
C_{sat}	Saturation concentration of S (sulfur) in the silicate melt (depending on the drop radius)
C_{sul}	Concentration of S in FeS melt (36.47 wt.%)
$C_{i,0}$, $C_{i,\infty}$	Concentration of element i in the initial and far-field silicate melt
$C_{i,sul}$	Concentration of element i in sulfide melt
D	Diffusivity of sulfur in silicate melt (sometimes D_S to distinguish it from D_i)
D_i	Diffusivity of element i in silicate melt
F	Remaining mass fraction of the silicate melt during crystal fractionation
F_d	Diffusivity factor (to adjust S diffusivity by multiplying F_d)
F_s	Solubility factor (to adjust S solubility by multiplying F_s)
F_{sil}	Mass of silicate melt divided by the mass of silicate + sulfide melts
F_{sul}	Mass of sulfide melt divided by the mass of silicate + sulfide melts
F_v	Viscosity factor (to adjust melt viscosity by multiplying F_v)
g	Acceleration due to Earth's gravity (9.8 m/s^2)
K_i	Partition coefficient of element i between sulfide and silicate melts
M_0	Initial mass of the silicate melt in which each sulfide droplet grows ($M_0 = \rho_{sil} / N$)
M_{sul}	Mass of the FeS melt droplet
N	Number density of sulfide nuclei (number per unit volume)
Pe	Peclet number (a dimensionless number defined as Pe $= 2aU / D$)
R	Universal gas constant (8.314 J K^{-1} mol^{-1})
S	Sulfide sulfur solubility (S concentration at sulfide saturation)
T	Temperature of the magma (in Kelvin unless otherwise noted)
T_0	The initial temperature of the magma, taken as the temperature when nucleation begins
T_∞	The final temperature of the system, taken to be 300 K
t	Time
U	Falling velocity of sulfide droplet in silicate melt
u	Growth rate of sulfide droplet in silicate melt
V_{sul}	Molar volume of FeS melt (21.7 × 10^{-6} m^3/mol)
V_0	Initial volume of silicate melt in which each sulfide droplet grows ($V_0 = 1 / N$)
w	Wt.% of H_2O in the silicate melt
x	Degree of oversaturation needed for nucleation to occur (Eq. (2))
β	A compositional parameter defined as: $\beta = (\rho_{sil} / \rho_{sul})(C_{sat} - C_\infty) / (C_{sul} - C_{sat})$
δ	Compositional boundary layer thickness for sulfur
δ_i	Compositional boundary layer thickness for element i
ΔM	Mass deficiency in the compositional boundary layer
η	Viscosity of silicate melt
ρ	Density
ρ_{sil}	Density of silicate melt (2760 kg/m^3)
ρ_{sul}	Density of sulfide melt (4050 kg/m^3)
σ	Interface tension between sulfide melt and silicate melt (0.5 N/m)
τ	Cooling time scale (Eq. (1)) of the magma, often taken to be 1000 to 10,000 yr

sulfur diffusivity (most likely decrease because sulfur diffusivity in basaltic melts decreases with viscosity increases, Behrens and Stelling, 2011). The quantitative relation between sulfur diffusivity and melt composition is not currently known. Increasing sulfur concentration and decreasing sulfide solubility in the melt would help the formation of sulfide deposits. Increasing viscosity and decreasing sulfur diffusivity will hinder the formation of sulfide deposits. Rough quantification of melt composition change is possible using the MELTS program (Ghiorso and Sack, 1995; Asimow and Ghiorso, 1998) by ignoring kinetics and dynamics of the crystallization process.

(ii) Crystal fractionation might deplete or enrich the ore elements (e.g., Simon et al., 2008; Simon and Ripley, 2011; Ripley and Li, 2013). In this work, only sulfide droplets are treated in detail, and the behavior of ore elements will only be considered parametrically in the Discussion.

(iii) The possibility for silicate and oxide crystals to serve as sites of sulfide droplet nucleation can be ruled out as Mungall and Su (2005) argued that heterogeneous nucleation of sulfide droplets is unlikely due to the very large contact angles that they measured between a sulfide drop immersed in silicate melt and alumina substrate.

(iv) The possibility that the droplets might stick to crystals and hence sink (or possibly even rise) with them can also be ruled out due to the large contact angles (Mungall and Su, 2005).

(v) As crystallinity increases, the magma may become more "rigid" for sulfide droplet settling, hindering sulfide deposit formation. However, the crystallinity of a slowly cooling magma cannot be easily predicted because crystals can settle, and the settling of crystals depends on the size and density of crystals as well as melt viscosity and cooling rate.

The problem of formation, growth and settling of each type of mineral has all the complexity of the problem of sulfide deposit formation to be modeled in this work, plus additional complexities of interacting grains (e.g., serving as nucleation sites, sticking together, and affecting the motion of one another). The presence of several kinds of minerals further complicates the inclusion of crystal fractionation in the modeling. Some of the effects help and other effects hinder sulfide deposit formation. Although the full treatment is not possible yet, a simplified treatment of the effect of crystal fractionation is presented below without the incorporation of the growth kinetics and settling dynamics.

3. Currently, no theory is available to allow accurate calculation of nucleation rate as a function of temperature and sulfur content. When they dealt with growth of multiple bubbles in explosive volcanic eruptions, Proussevitch and Sahagian (1998) started from a fixed number of bubbles to circumvent the need to treat nucleation. In this work, an empirical and approximate method is also used for nucleation rates, which represents the largest uncertainty in the modeling. It is assumed that there is one single nucleation event leading to N critical nuclei per m^3 once the degree of supersaturation reaches x (both N and x are parameters to be varied). Because it is known from crystal size distribution studies (e.g., Cashman and Marsh, 1988; Cashman, 1991; Bindeman, 2003) that crystal nucleation is continuous, the assumption of one-time event for the nucleation of sulfide droplets is clearly an oversimplification, which needs to be improved in the future. The degree of supersaturation x is defined as

$$x = (C/S)-1, \tag{2}$$

where C is the sulfur concentration (mass fraction) in the silicate melt, and S is the sulfur solubility in the melt. Therefore, given the initial sulfur concentration C_0 and a specified value of x for nucleation to occur, it means that nucleation occurs at temperature T_0 such that

$$S(T_0) = C_0/(1 + x). \tag{3}$$

From the above equation and given C_0, x, and the solubility relation, T_0 can be solved. This T_0 decreases as x increases, and is used in Eq. (1). The nucleus radius is the critical radius (e.g., by combining Eqs. 4-2c and 4-3 in Zhang, 2008) and is used as the initial radius a_0 of the droplets:

$$a_0 = 2\sigma V_{sul}/[RT_0 \ln(1 + x)] \tag{4}$$

where σ is the interface tension between sulfide melt and silicate melt, V_{sul} is molar volume of FeS melt (Kress et al., 2008) and R is the universal gas constant. When σ increases, the surface effect must be overcome by a larger droplet size to form a stable nucleus, accounting for the increase of a_0 with σ in Eq. (4). At T_0, N nuclei form per m^3, meaning that on average each droplet grows in a silicate

melt volume of $1/N$. Because the partial molar volume of FeS in the silicate melt is not known, a simplification is made by assuming that it is the same as the molar volume of FeS melt so that the total volume of the FeS droplets and the silicate melt does not change with the growth of the droplets. This simplification has only insignificant effect on the modeling results.

4. No experimental data are available to determine whether the falling of a sulfide droplet in a silicate melt follows the rigid sphere behavior or fluid sphere behavior. Sulfide drops are fluid spheres, and in theory fluid spheres have higher falling velocities, with 1.5 times the rigid sphere velocities at the maximum (Hadamard-Rybczynski equation, Clift et al., 1978). However, in practice, fluid spheres, such as bubbles in liquid, have often been found to behave as rigid spheres, often explained by the presence of surfactants (Levich, 1962; Shafer and Zare, 1991). The oil drop settling velocity data of Bremond d'Ars et al. (2001) are consistent with oil drops behaving as rigid spheres although data scatter does not allow affirmative conclusion. It is assumed in this model that a sulfide droplet behaves as a rigid sphere as it falls in the silicate melt. The falling velocity U is then calculated using Stokes' law because preliminary calculations show that the droplets are small and the Reynolds number is $\ll 1$:

$$U = 2ga^2(\rho_{sul}-\rho_{sil})/(9\eta), \tag{5}$$

where g is the acceleration due to Earth's gravity, a is the droplet radius, ρ_{sul} and ρ_{sil} are the densities of sulfide and silicate melts, and η is the silicate melt viscosity. (The Reynolds number Re is defined as the inertial force (or resistance to change) over viscous force. For the case of a sphere falling in a fluid, $Re = 2aU\rho / \eta$, where ρ and η are the density and viscosity of the silicate melt, respectively.) The assumption of rigid sphere behavior is not critical to the model and the maximum uncertainty of a factor of 1.5 is less than the uncertainty in parameters such as diffusivity and viscosity. Because sulfur concentration is low, meaning that sulfide droplets are typically separated far from each other, coalescence during droplet motion is not considered to be important. (Near the bottom of a magma chamber where sulfide drops accumulate, coalescence is important, but at that time sulfide drops are already at the bottom.)

5. As the magma cools further after droplet nucleation, the droplets continue to grow. The convective growth rate u is estimated as follows (Zhang et al., 1989; Kerr, 1995):

$$u = da/dt = \beta D/\delta, \tag{6}$$

where a is the droplet radius, D is the sulfur diffusivity in the silicate melt, β is a compositional parameter and δ is the effective thickness of the compositional boundary layer surrounding the droplet and can be calculated as (Kerr, 1995) for $Re \ll 1$:

$$\delta = 2a/\left[1 + (1 + Pe)^{1/3}\right], \tag{7}$$

where Pe is the compositional Peclet number defined as $Pe = 2aU / D$. The compositional parameter β in Eq. (6) is expressed as (Zhang, 2008, notes below Eq. (4)-125):

$$\beta = (\rho_{sil}/\rho_{sul})(C_\infty - C_{sat})/(C_{sul}-C_{sat}), \tag{8}$$

where C is the mass fraction, C_{sul} is the sulfur concentration in FeS melt (36.47 wt.%), C_∞ is the dissolved sulfur concentration in the far-field silicate melt and changes with time, and C_{sat} is the sulfur saturation concentration and depends on the radius of the drop because a small drop has high Gibbs free energy due to surface energy contribution. Assuming interface equilibrium, C_{sat} is the sulfur concentration in the interface silicate melt at $r = a$ and both can be expressed as (Zhang, 2008, Eq. (4)-76):

$$C_{sat} = C|_{r=a} = S\exp[2\sigma V_{sul}/(aRT)]. \tag{9}$$

In the experiments by Kerr (1995) and Zhang and Xu (2003) as well as the modeling by Zhang (2005) and Zhang and Xu (2008), the value of C_∞ can be and was treated as a constant. However, here, the value of C_∞ decreases with sulfide droplet growth, and is estimated from the initial sulfur concentration minus sulfur that went into sulfide droplets and sulfur deficiency in the boundary layer as follows:

$$C_\infty = \frac{C_0 - \frac{M_{sul}}{M_0}C_{sul} - \frac{\Delta M}{M_0}}{1-\frac{M_{sul}}{M_0}}, \tag{10}$$

where $M_0 = \rho_{sil}V_0 = \rho_{sil} / N$ is the average silicate melt mass per sulfide droplet, $M_{sul} = (4\pi a^3 / 3)\rho_{sul}$, C_0 is the initial sulfur mass fraction in the silicate melt, and ΔM is the amount of sulfur depletion in the boundary layer (ΔM is negative for sulfur depletion and usually negligible).

6. Zhang and Xu (2003) discussed that if the composition varies significantly across the boundary layer in terms of major elements, the variation of viscosity, density and diffusivity across the boundary layer would cause additional errors in the model calculation. Because sulfide solubility is small in silicate melts, the melt composition across the boundary layer does not vary much. Hence, this is not a source of modeling errors.
7. Magma convection in the magma body is expected to affect the motion of individual sulfide droplets. However, the convective growth rate is controlled by the boundary layer thickness around a moving droplet and is not much affected by the bulk convection in the magma body. For example, Walker and Kiefer (1985) showed that increased turbulence due to bulk flow does not increase the dissolution rate of falling salt crystals in water. The bulk upward and downward flow can entrain the sulfide droplets and hence change the time for individual droplets to fall to the bottom. However, because upward flow is balanced by the downward flow in a convection cell, the average time for a droplet to sink would roughly stay the same even in the presence of convection. That is, the bulk convection does not significantly affect the average behavior of sulfide droplets, which is modeled in this work.
8. The vertical temperature gradient in the magma body is ignored. Assuming the magma chamber is adiabatic, the temperature gradient would be about 1 K per km using heat capacity of Lange and Navrotsky (1992) and melt density and thermal expansivity of Lange and Carmichael (1990) and Ochs and Lange (1997). Because the default magma chamber thickness is 1 km, the temperature variation would only have a negligible effect on the model. The sulfide saturation temperature for a given sulfur content also depends slightly on depth, about 3 K per km using Li and Ripley (2009), also a negligible effect.

In summary, the growth rate of a sulfide droplet is calculated from Eq. (6) and the settling velocity is calculated from Eq. (5). The radius as a function of time is calculated by integration of the growth rate. The settling distance as a function of time is calculated by integration of the settling velocity with respect to time. The calculation is carried out numerically and iteratively. The largest uncertainty in the model that will need to be improved in the future is on the quantification of sulfide droplet nucleation rate as a function of sulfur content, temperature, pressure, melt composition (including H_2O content), and crystallinity. Other factors that need to be considered in modeling specific sulfide deposits include specific cooling history, crystal fractionation, assimilation and magma mixing. The assumption that sulfide droplets behave as rigid spheres is not critical.

3. Input parameters

Important parameters to model the processes include: sulfide and silicate melt composition, the viscosity of silicate melt η, the solubility of sulfur in silicate melt S, the diffusivity of sulfur in silicate melt D, interface tension between sulfide melt and silicate melt σ, and density of sulfide and silicate melts. The parameters are discussed and evaluated below.

1. The sulfide melt composition is assumed to be FeS for the calculation of sulfide melt density, sulfide melt molar volume, interface tension between sulfide melt and silicate melt, and sulfur solubility in the silicate melt.
2. In this work, dry Etna basalt composition (Table 2) is used as the starting silicate melt composition because for this melt, the important melt properties have been measured so that realistic simulations can be carried out. As will be shown below, sulfur diffusion data are limited and no general diffusivity model is available for different melt compositions. Because it is desirable to maintain self-consistency in the input parameters, the decision is made to use Etna melt composition for which sulfur diffusion data are directly available. Both viscosity and sulfur diffusivity have been directly measured for dry Etna basaltic melt (Giordano and Dingwell, 2003; Freda et al., 2005). The availability of viscosity data for Etna basaltic melt provides better constraints on viscosity than can be calculated from general viscosity models. The solubility model of Li and Ripley (2009) is used to calculate sulfur solubility in Etna basalt (average of the two Etna basalt compositions by Giordano and Dingwell, 2003 and Freda et al., 2005).
3. Melt viscosity. A vast literature is available with thousands of viscosity data for natural silicate melts covering a wide range of temperature, pressure, and melt composition including H_2O content (e.g., Bottinga and Weill, 1972; Shaw, 1972; Richet, 1984; Richet et al., 1996; Schulze et al., 1996; Whittington et al., 2000; Giordano and Dingwell, 2003; Zhang et al., 2003; Hui and Zhang, 2007; Zhang and Xu, 2007; Giordano et al., 2008; Hui et al., 2009; Whittington et al., 2009; Misiti et al., 2011). Two general models (Hui and Zhang, 2007; Giordano et al., 2008) have been developed that are intended to predict natural silicate melt viscosity for essentially any melt composition and at essentially all conditions (except for high pressures) in the viscosity range of $\leq 10^{15}$ Pa·s. However, the precision of the general models is not very high. For example, the 2σ uncertainty in predicting $\log\eta$ is 0.61 units for both dry and hydrous melts for the model of Hui and Zhang (2007) and 0.5 to 0.7 units for dry to hydrous melts for the model of Giordano et al. (2008). There are models for specific melt compositions with higher accuracy such as 2σ uncertainty of 0.3 $\log\eta$ units (e.g., Schulze et al., 1996; Zhang et al., 2003; Whittington et al., 2009; Misiti et al., 2011). The viscosity of Etna basaltic melt has been directly measured as a function of temperature and H_2O content by Giordano and Dingwell (2003). For the anhydrous melt (with 0.02 wt.% H_2O), the temperature range covered by the viscosity data is 985 to 1818 K. However, for hydrous Etna basalt, the viscosity data only covered temperatures $\leq$ 893 K. Hence, only the dry melt viscosity data are fit as a non-Arrhenian function of temperature as follows:

$$\eta = \exp\left[-4.476 + (3100/T)^{2.952}\right], \quad (11)$$

where η is the viscosity in Pa·s and T is the temperature in Kelvin. The 2σ uncertainty of the above equation in predicting dry Etna basalt viscosity is 0.07 $\log\eta$ units.
4. Sulfur diffusion data in silicate melts of geological interest are limited (Watson, 1994; Baker and Rutherford, 1996; Winther et al., 1998; Freda et al., 2005) and have been reviewed by Zhang et al. (2007, 2010) and Behrens and Stelling (2011). The only S diffusion data in mafic melts are by Freda et al. (2005) using Etna basalt and Stromboli basalt. As shown in Table 3, even though the two basalts are only subtly different in composition, and even though the viscosity of Etna basalt (Giordano and Dingwell, 2003) differs little from that of Stromboli basalt (Misiti et al., 2009), S diffusivity in Etna basalt is 3 times that in Stromboli basalt (Freda et al., 2005). Because no general S diffusivity model accounting for the compositional dependence is available and because S diffusivity can vary significantly even when the compositional variation is small, there is a critical need to investigate S diffusion in various melts for modeling the formation of specific sulfide deposits. Without such data, one very rough approximation is to assume that S diffusivity in basaltic and andesitic melts is Eyring (Behrens and Stelling, 2011), meaning that $D = k_B T/(\lambda\eta)$, where k_B is the Boltzmann constant, and λ is the sulfur atomic/ionic jumping distance. As shown by Behrens and Stelling (2011), S diffusivity differs from the Eyring diffusivity by no more than a factor of 10 (still large) for basaltic and andesitic melts, but the difference can be a factor of 10^6 for rhyolitic melts.
Using the experimental data of Freda et al. (2005), sulfur diffusivity in Etna basalt as a function of temperature and H_2O content at 0.5 to 1.0 GPa can be fit as

$$D = \exp[-8.787-(25774 - 429w)/T], \quad (12)$$

where D is in m^2/s, and w is H_2O wt.% (0.5 wt.% means $w = 0.5$).
5. The solubility of sulfur in silicate melts, that is, the sulfur concentration at sulfide saturation, has been investigated extensively (e.g., Naldrett, 1969; Haughton et al., 1974; Shima and Naldrett, 1975; Buchanan and Nolan, 1979; Carroll and Rutherford, 1987; Luhr, 1990; Peach and Mathez, 1993; Peach et al., 1994; Gaetani and Grove, 1997; Mavrogenes and O'Neill, 1999; O'Neill and Mavrogenes, 2002; Holzheid and Grove, 2002; Satari et al., 2002; Jugo et al., 2005; Scaillet and MacDonald, 2006; Liu et al., 2007; Brenan and Haider, 2008; Jugo, 2009). General models have also been constructed to predict sulfur solubility in silicate melts of various compositions (e.g., Mavrogenes and O'Neill, 1999; Holzheid and Grove, 2002; Li and Ripley, 2005; Moretti and Otonnello, 2005; Liu et al., 2007; Moretti and Baker, 2008; Jugo, 2009; Li and Ripley, 2009; Baker and Moretti, 2011). Based on data and models, sulfur solubility in silicate melts increases with increasing temperature and FeO content, and decreases with increasing pressure and SiO_2 content. For this work, the sulfur solubility is calculated using the model of Li and Ripley (2009), whose complete equation is (Eq. (16) in their paper):

$$\ln X_S = -1.76-4740/T-0.0021P + 5.559X_{FeO} + 2.565X_{TiO_2} + 2.709X_{CaO}-3.192X_{SiO_2}-3.049X_{H_2O},$$

Table 2
Etna basalt composition (normalized to 100 wt.%).

	SiO_2	TiO_2	Al_2O_3	FeO_t	MnO	MgO	CaO	Na_2O	K_2O	P_2O_5
Etna1	48.40	1.66	16.75	10.43	0.21	5.32	10.77	3.86	2.00	0.61
Etna2	47.72	1.74	16.79	11.00	0.18	6.38	10.74	3.19	1.72	0.55
Ave	48.06	1.70	16.77	10.71	0.19	5.85	10.76	3.52	1.86	0.58

Etna1 is from Giordano and Dingwell, 2003; Etna2 is sulfur-rich Etna basalt of Freda et al., 2005. Ave is average of Etna1 and Etna2. The calculated liquidus for the dry Etna basalt (average composition) at QFM is 1468 K at 200 MPa and 1516 K at 500 MPa using MELTS (Ghiorso and Sack, 1995; Asimow and Ghiorso, 1998).

Table 3
Chemical composition, viscosity and S diffusivity of two basaltic melts.

Melt	SiO_2	TiO_2	Al_2O_3	FeOt	MgO	CaO	Na_2O	K_2O	P_2O_5	logη	log$D$
Etna	47.72	1.74	16.79	11.00	6.38	10.74	3.19	1.72	0.55	1.60	−11.18
Stromboli	50.78	0.94	18.47	6.38	6.35	12.20	2.43	1.89	0.38	1.69	−11.66

Note: Compositions are from Freda (2005). Viscosity (η, in Pa·s) and S diffusivity (D, in m^2/s) are for dry Etna and Stromboli melts at 1523 K (Giordano and Dingwell, 2003; Freda et al., 2005; Misiti et al., 2009).

where P is in GPa and X is mole fractions. For the specific composition of Etna basalt at $P = 0.5$ GPa, sulfur solubility in wt.% can be simplified to:

$$S = \exp(1.303 - 4740/T - 0.055w). \quad (13)$$

where S is the sulfur concentration in wt.% at sulfide saturation.

6. The density of silicate melt has been investigated extensively, and Lange and Carmichael (1990) and Ochs and Lange (1997) developed models for density calculation. Silicate melt density depends on temperature, pressure, and H_2O content. Furthermore, as the FeS component is removed to the sulfide droplets, silicate melt density is also expected to vary. On the other hand, the density variation is relatively small, whereas incorporation of the variation of density would make the treatment much more complicated. For example, Eqs. (6) and (8) are derived for constant density of silicate and sulfide melts. Incorporating density variation would complicate the equations in a major way and the gain is minimal. Hence, a constant density of 2760 kg/m^3 for dry Etna melt (1473 K and 0.5 GPa) is adopted. This approximation is expected to have only insignificant effect on the modeling results.
7. Sulfide melt density has also been measured (Kress et al., 2008) and density variation of FeS melt with temperature and pressure is also readily available (e.g., Kress et al., 2008). Again, to avoid complexity associated with variable sulfide melt density, a constant sulfide melt density of 4050 kg/m^3 is adopted. This approximation is expected to have only a small effect on the modeling results.
8. Mungall and Su (2005) measured the interface tension between FeS melt and basalt melt to be 0.5 N/m at 1250–1275 °C. The interface tension is expected to depend on temperature and the compositions of both the sulfide and silicate melts, but no quantification is available.

4. Modeling results

Model calculations have been carried out to examine the effect of various parameters. The calculation is first done for a specific melt (dry Etna basalt) in Section 4.1 using the appropriate melt viscosity and density, and sulfur diffusivity and solubility in the basaltic melt so that the modeling is realistic rather than parametric. The parameters to be explored for Etna basalt include the degree of supersaturation needed for nucleation (x), the number of nuclei at this degree of supersaturation (N), the cooling time scale (τ), the initial sulfur concentration, and the settling distance. Most of the simulation results are expressed as the required initial sulfur concentration (C_0) to achieve a settling distance of 1 km given x, N and τ. The choice of 1 km is arbitrary (e.g., Marsh, 1989) and is related to the typical crustal magma chamber thickness which is of the order 0.1 to 10 km with a median of 1 km. This required C_0 is interpreted to be the critical initial C_0 to produce sulfide deposits. In Section 4.2, the effect of melt viscosity and sulfur solubility and diffusivity (i.e., for melts with different melt composition including different H_2O contents) is explored parametrically because no actual data are available for realistic evaluation. In Section 4.3, the effect of crystal fractionation is discussed.

4.1. Modeling results for dry Etna basalt

In this section, results on sulfide droplet growth and settling in dry crystal-free Etna basaltic melt are presented because viscosity and diffusivity in the melt are known. (It is not difficult to model wet basaltic melts when the relevant data are available.) First, the effect of x and N on droplet growth and settling and the relation between initial concentration and settling distance are examined. Then, summary results are presented to evaluate the required initial sulfur concentration (C_0) to achieve a settling distance of 1 km given x, N and τ.

4.1.1. Effect of x (degree of supersaturation)

Calculated droplet growth and settling as a function of the degree of supersaturation are shown in Fig. 3. From Fig. 3a, when the degree of supersaturation required for nucleation to occur is small (e.g., $x = 0.001$), the initial droplet growth is not significant and the radius vs. time curve is smooth. On the other hand, if the degree of supersaturation required for nucleation to occur is large (e.g., $x = 0.2$), each newly formed sulfide droplet grows in a highly supersaturated silicate melt, leading to rapid initial growth (i.e., the steep rise of the r vs. t curve in blue in Fig. 3a) to roughly reach equilibrium between the silicate melt and the sulfide droplet. The common occurrence of sulfide drops in mid-ocean ridge basaltic glasses (e.g., Wallace and Carmichael, 1992) implies that the degree of supersaturation required for nucleation to occur is not very large, but quantification is not possible at present. After the rapid growth, the droplet grows slowly. The final droplet size does not depend much on x for this example because the cooling time scale is relatively long for the given number of droplet nuclei so that there was near equilibrium at high temperature and hence the final size does not depend on initial conditions. If τ and N are significantly reduced, then the final droplet size would decrease with increasing x because there would not be enough time to achieve near equilibrium even at high temperature.

The settling distance versus time is shown in Fig. 3b. The final settling distance decreases as x increases (Fig. 3b) even though the final drop radius is almost identical (Fig. 3a). The effect of varying x on settling distance is not very large (less than a factor of 3) and can be explained as follows. When x is small, the nucleation temperature (T_0, shown in Fig. 3) is high, meaning lower viscosity and higher descending velocity of the droplet. When x is large, the droplet forms at a lower temperature, meaning high viscosity, and smaller droplet settling velocity.

4.1.2. Effect of N (number density of nuclei)

Fig. 4 shows the growth and settling as a function of time for different numbers of nuclei (N). As N increases, each sulfide droplet grows in a smaller volume of silicate melt, resulting in a smaller final droplet size, and also a smaller settling distance. When the droplet number density decreases by a factor of 10, the final radius increases by almost the theoretical factor of $10^{1/3} \approx 2.15$, and the settling distance increases by a factor of $<10^{2/3} = 4.64$.

4.1.3. Relation between the initial S content and settling distance

Fig. 5 examines the relation between initial S concentration and settling distance. For a given set of conditions, higher initial S concentration means greater settling distance, as expected. Quantitatively, for the settling distance to increase from 0.1 km to 10 km (2 orders of magnitude

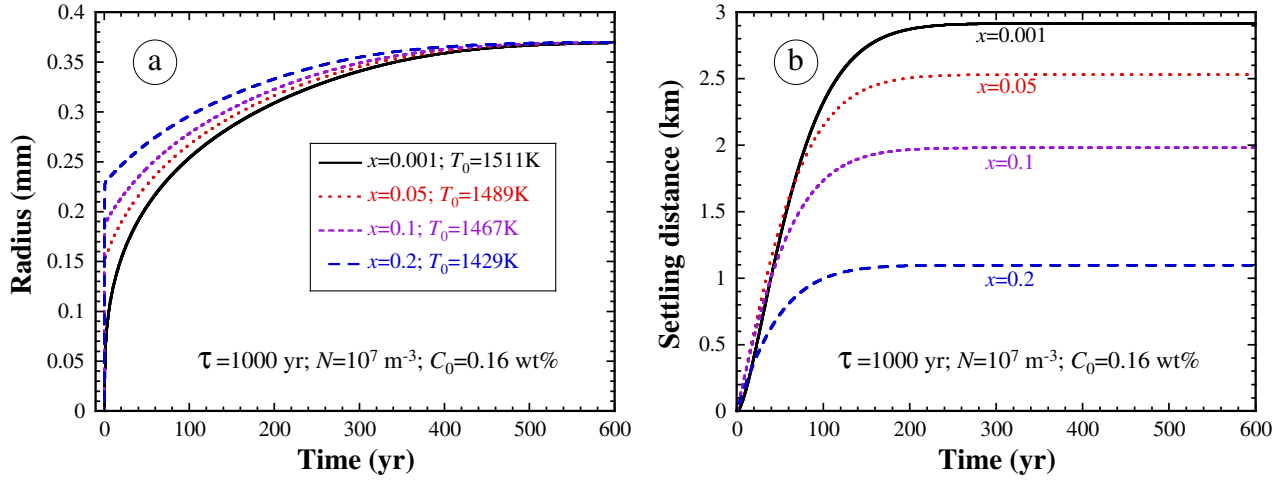

Fig. 3. The growth and settling of sulfide droplet with time at various degrees of supersaturation *x*. The temperature at the time of nucleation is given in the legend. (For interpretation of the references to color in this figure, the reader is referred to the web version of this article.)

essentially covering all realistic settling distances in ore-forming magma chambers), the required C_0 needs to increase by 20% to 60% depending on other conditions.

In the following simulations, the default of the settling distance (h) is 1 km, and the results are expressed as the required initial S concentration for droplets to settle this distance. The calculated required initial S concentration is referred to as the critical initial S concentration for sulfide segregation.

4.1.4. Required C_0 as a function of x

Fig. 6 shows the relation between the required C_0 and x at fixed τ and N (and $h = 1$ km hereafter). Increasing the degree of supersaturation at which nucleation occurs makes it more difficult to produce sulfide melt droplets and hence more difficult to produce sulfide deposits, meaning increased C_0. This expectation is confirmed by the model calculations. Furthermore, Fig. 6 shows that the required C_0 is almost linear to x (more accurately linear to $x^{1.14}$).

4.1.5. Required C_0 as a function of N

Fig. 7 displays how C_0 depends on N. Increasing the number of nuclei when the degree of supersaturation reaches the set value leads to smaller droplets and smaller settling velocity, and hence more difficulty in forming sulfide deposits. That is, higher initial S concentration would be needed to form ores. The results in Fig. 7 confirm this expectation. Quantitatively, C_0 is approximately linear to $N^{0.13}$ at $\tau = 1000$ yr and $\tau = 10{,}000$ yr. Furthermore, when the number of nuclei is large, diffusion distance is short, the growth is almost near equilibrium growth, and diffusivity plays a less important role.

4.1.6. Required C_0 as a function of τ

Fig. 8 illustrates that the required C_0 decreases with increasing cooling time scale τ. This is expected because with slower cooling, there is more time for sulfide droplet growth and settling, and hence formation of sulfide deposits is more likely.

4.1.7. Summary of modeling results

The modeling results show that in a dry melt of Etna basalt composition, a segregated sulfide-rich layer would form when the initial sulfur concentration is about 0.10 to 0.30 wt.%, and the exact value depends on other conditions. These concentrations are similar to sulfur contents in natural mantle-derived basaltic melts. For example, Wallace and Carmichael (1992) reported sulfur concentration in various mid-ocean ridge basalts ranging from 0.10 to 0.25 wt.% S. The similarity demonstrates that (i) my physical model considering the thermodynamics, kinetics and dynamics of sulfide deposit formation using real magma properties is likely applicable to sulfide deposition formation in common natural settings, and (ii) many mafic magmatic bodies are capable of forming sulfide deposits if the cooling time scale is long (large magma

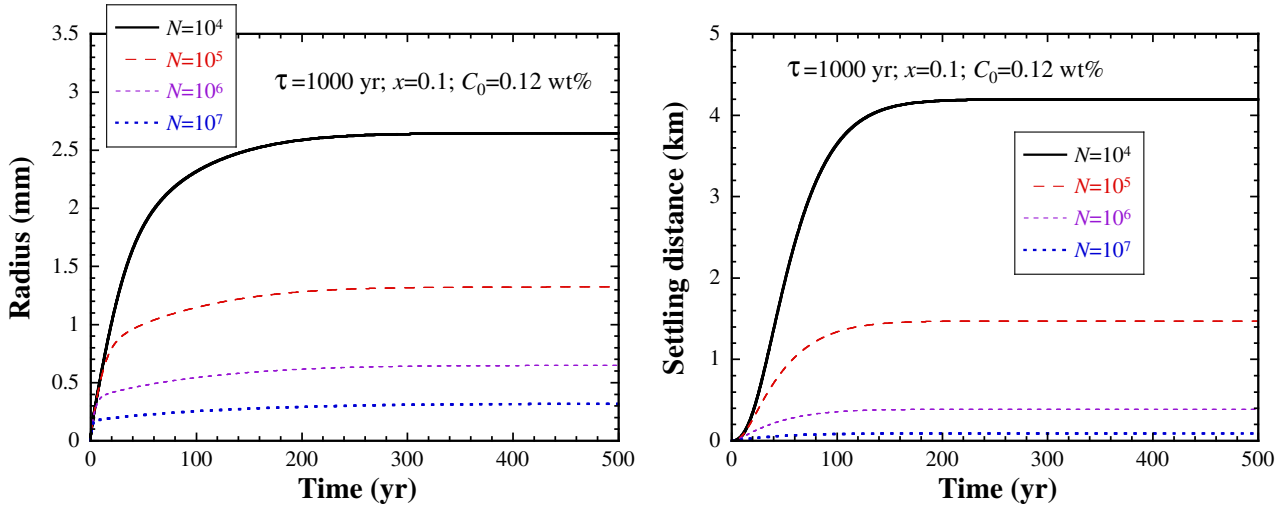

Fig. 4. The growth and settling of sulfide droplet with time at various numbers of nuclei at nucleation. The unit of N is m^{-3}. For the simulations, $T_0 = 1347$ K, and at $t = 100$ yr, $T = 1247$ K.

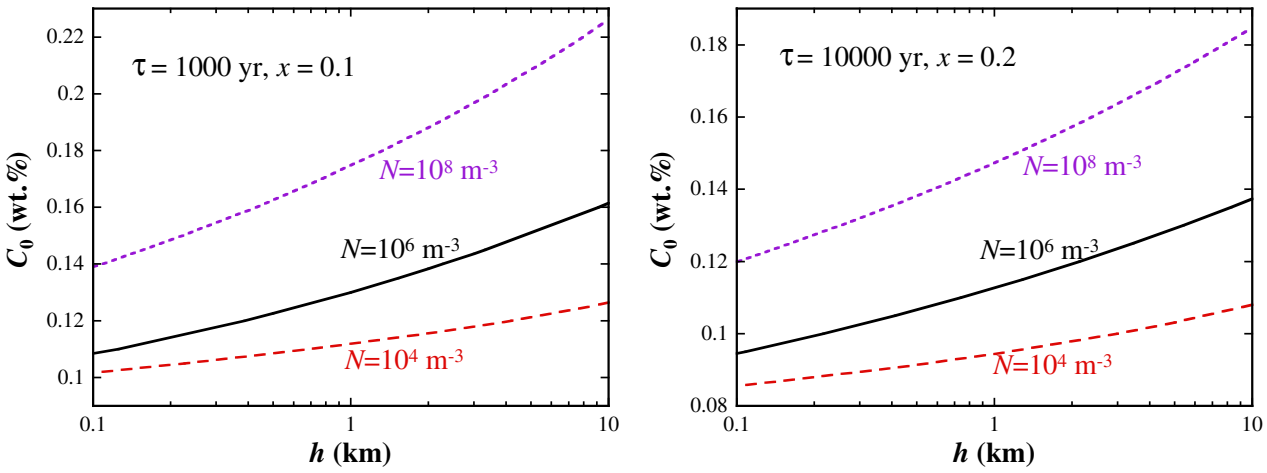

Fig. 5. The dependence of the critical initial S concentration on the required settling distance for Etna basalt melt with cooling time scales of 1000 yr and 10,000 yr.

body). For a given magma body, the settling distance can be gauged from the size of the magma body, and the cooling time scale may be independently estimated by thermal modeling of the magma body. Magma properties such as melt viscosity and sulfur solubility are increasingly better constrained by experiments and modeling. Sulfur diffusivity can be experimentally studied. Initial S concentration may be estimated from melt inclusion studies. The most uncertain parameters are the nucleation parameters x and N, whose effects are examined in Figs. 6 and 7. It is hoped that theoretical progress in the future will help constrain the nucleation rates.

4.2. Effect of viscosity, sulfur solubility and diffusivity

If the melt composition is different from that of Etna basalt, the melt viscosity, and sulfur solubility and diffusivity will all change. Because sulfur solubility depends strongly on FeO concentration but viscosity and diffusivity do not, the solubility variation is not always well correlated with viscosity variation. On the other hand, Behrens and Stelling (2011) showed that when viscosity is less than 10^4 Pa·s, sulfur diffusivity roughly follows the Eyring diffusivity (but the scatter is about an order of magnitude) for natural silicate melts, meaning that sulfur diffusivity is roughly inversely proportional to viscosity. For Etna basalt, sulfur diffusivity by Freda et al. (2005) is only slightly larger than (3.1 to 4.6 times) the Eyring diffusivity calculated using viscosity data of Giordano and Dingwell (2003) at 1573 to 1473 K. As the melt cools (with or without crystal fractionation), the departure from the inverse correlation between diffusivity and viscosity increases, but the growth and descent of sulfide drops becomes insignificant at lower temperatures. Due to the lack of sulfur diffusion data in natural melts and in order to simplify the simulations, sulfur diffusivity is assumed to inversely co-vary with melt viscosity although it is known that such a relation is not accurate. If diffusivity is allowed to change independently, for small N ($<10^6$ m^{-3}), increasing or decreasing the diffusivity by a factor may lead to a similar factor change in the settling distance. If N is large, then the effect of changing D does not affect the results much.

In the following simulations, the effect of viscosity and solubility is examined parametrically by varying each parameter by a factor denoted as F_v (viscosity factor) and F_s (solubility factor). Sulfur solubility does not vary tremendously with composition and F_s will be allowed to vary from 0.25 to 2. On the other hand, melt viscosity can vary easily by several orders of magnitude, and F_v will be allowed to vary from 0.1 to 1000 in the simulations. The diffusivity factor F_d is set to be $1/F_v$ in the simulations as discussed above.

The dependence of the critical initial sulfur concentration in the melt for the sulfide drops to settle by 1 km on the solubility factor is simple and is shown in Fig. 9. The relation is almost proportional, which is understandable because increasing solubility can be compensated by increasing the initial concentration required for the formation of sulfide drops. However, the compensation is not exact because higher initial concentrations mean more rapid droplet growth. The simulation

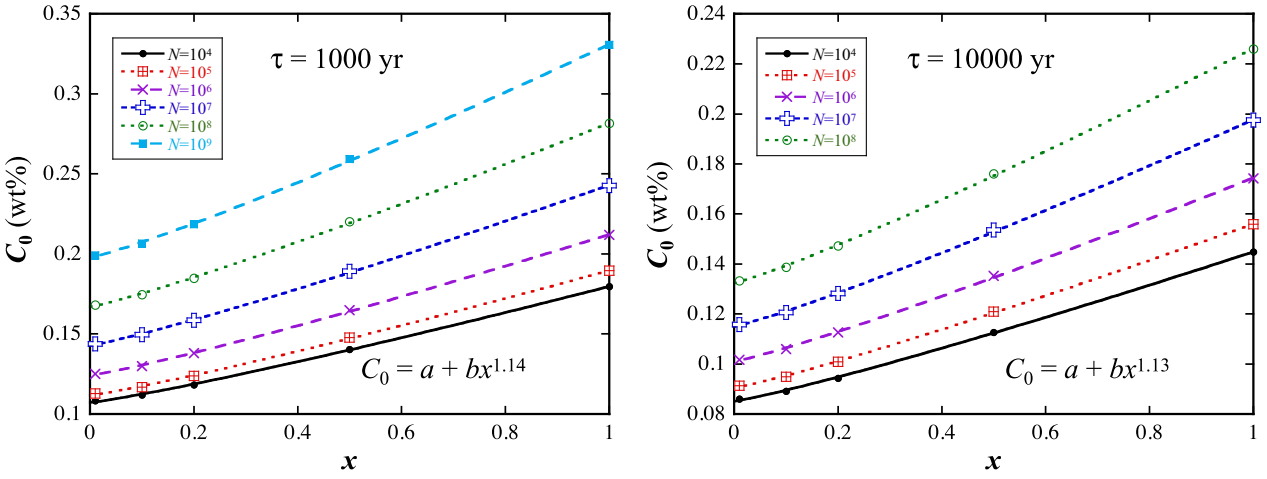

Fig. 6. The dependence of the critical initial sulfur concentration (C_0) on the degree of supersaturation (x) for different numbers of nuclei at cooling time scale of 1000 yr and 10,000 yr. The settling distance is 1 km.

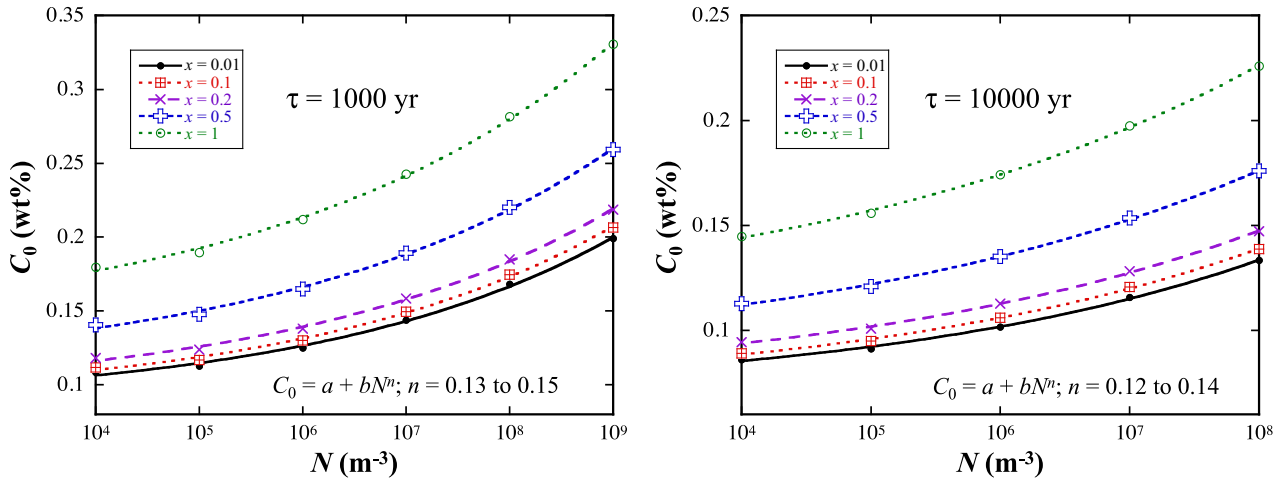

Fig. 7. The relation between the critical initial sulfur concentration (C_0) and the number density of nuclei in the melt. The settling distance is 1 km.

shows that the critical C_0 is roughly proportional to the solubility factor raised to 0.935th power.

Fig. 10a shows how the critical initial sulfur concentration is related to F_v. It is found that if τ/F_v ($=\tau F_d$) is used as the horizontal axis, all the different curves in Fig. 10a collapse exactly into a single curve as shown in Fig. 10b. That is, the correlated viscosity increase and diffusivity decrease are exactly compensated by cooling time scale increase. The compensation can be proved as follows. Given an increase in viscosity by a factor of F_v, meaning new viscosity $\eta = F_v\eta_0$ where the subscript "0" stands for the original condition, and new diffusivity $D = F_dD_0 = D_0 / F_v$, if the cooling time scale increases by a factor of F_v, meaning $t = F_vt_0$, then: the falling velocity U is decreased by the viscosity factor $U = U_0 / F_v$ according to Stokes' law (Eq. (5)) because the flow is creeping flow, the diffusion distance $(\int Ddt)^{1/2} = [\int(D_0 / F_v)d(F_vt_0)]^{1/2} = (\int D_0dt_0)^{1/2}$, and the falling distance $\int Udt = \int(U_0 / F_v)(F_vdt_0) = \int U_0dt_0$. That is, the new falling velocity, diffusion distance and falling distance are the same as the original, meaning that there is exact compensation. The proof also shows that if η and D do not co-vary inversely, the effect cannot be completely compensated by a change in the cooling time scale.

More simulation data for the relation between C_0 and τF_d are shown in Fig. 11. By fitting the data C_0 is roughly linear to $(\tau F_d)^{-1/6}$. This result at first seems to contradict Fig. 8 where C_0 is roughly linear to $\tau^{-0.14}$. This difference turns out to be due to the large spread in τF_d (7 orders of magnitude) in Fig. 11 compared to the smaller spread of τ (3 orders of magnitude) in Fig. 8. If in Fig. 11, the range of τF_d is limited to 100 to 100,000, then an exponent of 0.13 to 0.14 will be obtained. This shows that the function that is adopted to fit the simulation results is not perfect.

4.3. Effect of crystal fractionation

As discussed earlier, the full kinetics and dynamics of crystal fractionation are impossible to model at present. In this section, a simple treatment of the effect of crystal fractionation is presented. In the treatment, crystals are assumed to grow and settle rapidly (i.e., growth kinetics and settling dynamics are ignored) compared to sulfide droplets. This is partially justified for major minerals such as olivine, pyroxenes and plagioclase because the growth of such minerals does not require depletion of a large region of the melt and hence equilibrium is more readily achieved, but is not well justified for chromite and apatite because Cr and P are also minor elements and mass transfer is expected to play some role in the growth.

With the assumption of rapid crystal growth and settling, it is possible to use the MELTS program (Ghiorso and Sack, 1995; Asimow and Ghiorso, 1998) to estimate the fractionated melt composition as a function of temperature. When the cooling function $T(t)$ is prescribed for modeling sulfide deposit formation, this means that melt composition as a function of time can also be obtained. S concentration is calculated assuming perfect incompatibility, meaning a partition coefficient of zero. Melt viscosity and S solubility can be calculated at the new melt composition. S diffusivity is not known as a function of melt

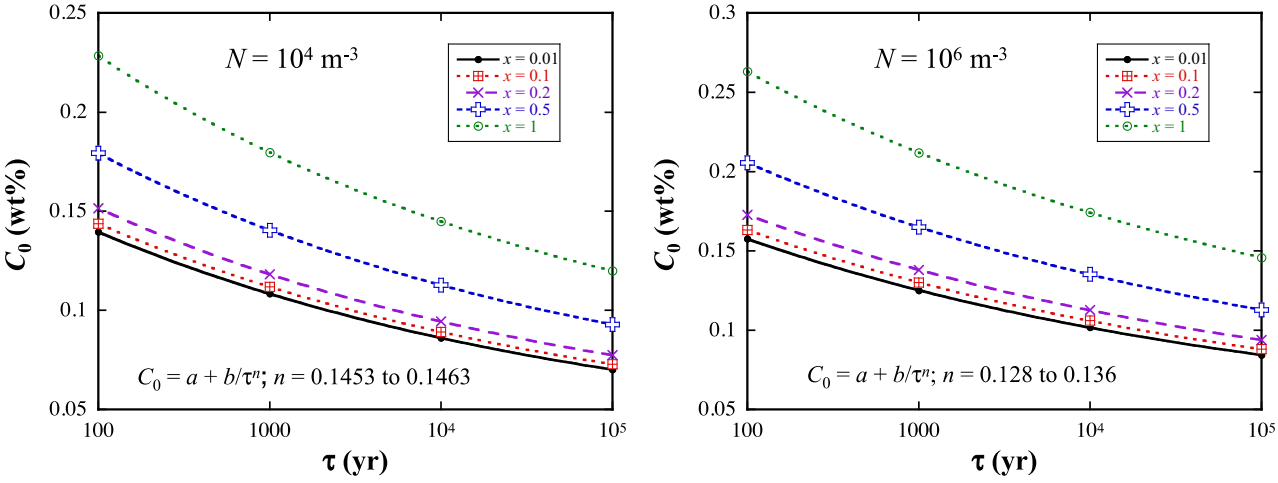

Fig. 8. The relation between the critical initial sulfur concentration (C_0) and the cooling time scale of the magma body. The settling distance is 1 km.

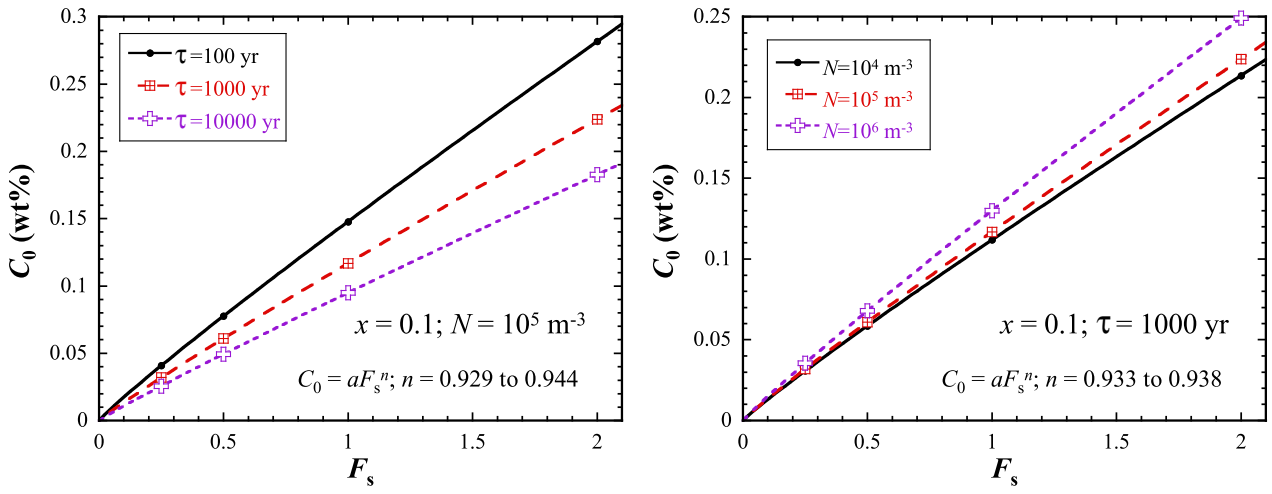

Fig. 9. The relation between the critical initial sulfur concentration (C_0) and the solubility factor F_s. The settling distance is 1 km.

composition and is estimated roughly assuming that it is inversely proportional to melt viscosity (Behrens and Stelling, 2011).

Fig. 12 shows the variation of melt mass fraction with temperature during fractional crystallization of liquid with the composition of Etna basalt calculated at 0.5 K temperature interval at 200 MPa and QFM. The liquidus temperature is 1468 K. The mass fraction of the melt changes gradually from 1 to 0.59 as temperature decreases from 1468 to 1402 K. Then, the melt fraction suddenly drops from 0.59 to 0.49 as temperature decreases to by 0.5 K, which is similar to a multicomponent eutectic when spinel joins the crystallizing phases and large quantities of spinel, clinopyroxene and plagioclase crystallize. From 1401.5 K to 1352 K, the melt fraction gradually decreases from 0.49 to 0.26. Then leucite joins the crystallizing phases and there is a slope change in the F vs T curve. The results are fit by the following piecewise and continuous function of $F(T)$ describing the mass fraction F of the melt as a function of temperature T:

$F(T) = 1$ when $T \geq 1468$ K
$F(T) = \exp[0.008(T - 1468)]$ when $1402 \leq T \leq 1468$ K
$F(T) = 0.487320681 + 0.204925354\,(T - 1401.5)$ when $1401.5 \leq T \leq 1402$ K
$F(T) = 0.487320681\exp(0.0124(T - 1401.5))$ when $1352 \leq T \leq 1401.5$ K
$F(T) = 0.359\exp[-0.1541(1356 - T)^{1/2}]$ when $T \leq 1352$ K.

The fit is shown as the red solid curve in Fig. 12a. Effort is made so that the above piecewise function is continuous at every point. S solubility as a function of temperature and melt composition is calculated at each temperature and is fit piecewise (Fig. 12b). The S concentration in the far-field melt (C_∞) without sulfide formation is C_0/F. Considering sulfide formation, the far-field S concentration can be obtained from Eq. (10) by replacing the value "1" in the denominator by F.

For melt viscosity at each temperature using the fractionated melt composition, when different models (Shaw, 1972; Hui and Zhang, 2007; Giordano et al., 2008) are used, diverging trends with complicated shapes are obtained even after the high temperature viscosity is adjusted to be consistent with Giordano and Dingwell (2003). A smoothed viscosity curve for fractionated melts is used with adjustment so that viscosity is consistent with Eq. (11) for the unfractionated melt. For S diffusivity, because no model is available to evaluate its variation as a function of melt composition, Eq. (12) is used. The uncertainty in the viscosity and especially the diffusivity may be large and cannot be evaluated accurately.

In carrying out the calculations, care was taken so that the piecewise function does not cause numerical trouble. Calculations show that when the initial sulfur concentration is high so that sulfide droplets form at much higher temperature than the beginning of crystallization, the effect of incorporating fractional crystallization is small. On the other hand, if the initial sulfur concentration is low so that sulfide droplets form after crystallization, the effect of incorporating fractional

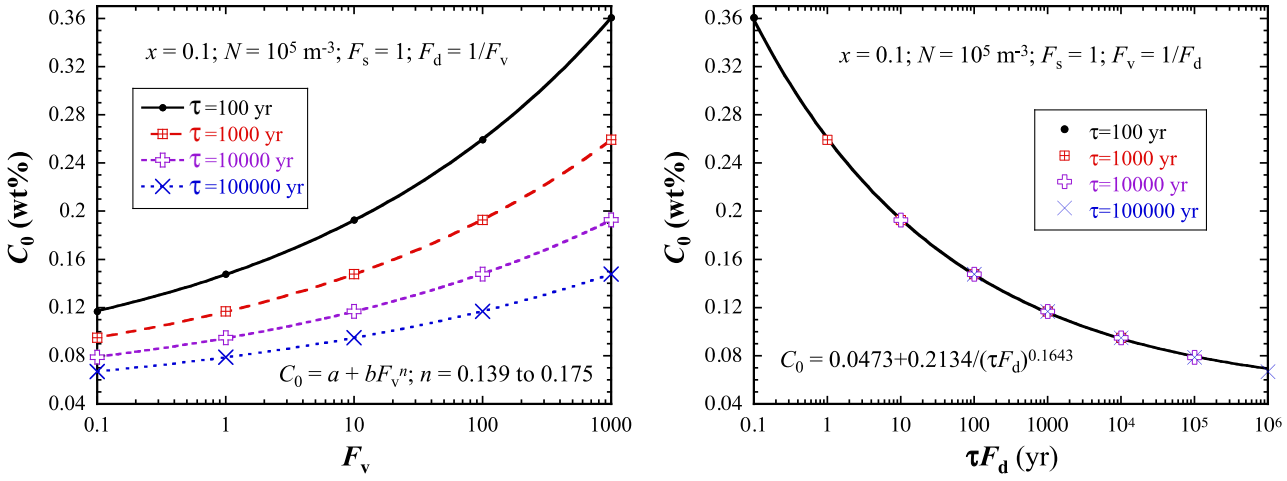

Fig. 10. The relation between the critical initial sulfur concentration (C_0) and the viscosity factor F_v and $\tau/F_v = \tau F_d$. The settling distance is 1 km.

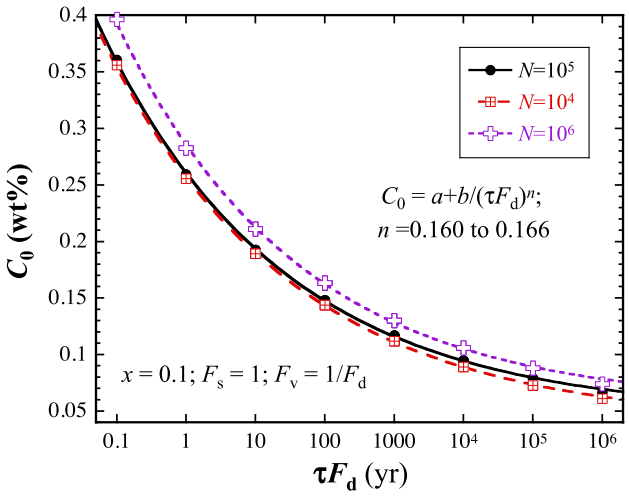

Fig. 11. The relation between the critical initial sulfur concentration (C_0) and the solubility factor F_v and $\tau/F_v = \tau F_d$. For the simulations, melt viscosity $\eta = F_v\exp[-4.476 + (3100/T)^{2.952}]$, sulfur diffusivity $D_S = F_d\exp(-8.787\text{–}25{,}774/T)$ with $F_d = 1/F_v$, and sulfur solubility $S = \exp(1.303\text{–}4740/T)$. The settling distance is 1 km.

crystallization is large due to increasing S concentration in the melt, resulting in sulfide droplet formation at a higher temperature. One comparison to demonstrate the large effect is shown in Fig. 13. The sulfide drop radius when crystal fractionation is considered increases only by 19% but the settling distance is 3 times that without considering crystal fractionation; the large difference in the settling distance is due to the formation of sulfide drop at a higher temperature and hence lower viscosity.

If the crystallized minerals are assumed to stay in the magma without settling, then the minerals would increase the viscosity, and the settling distance may become smaller than without crystallization. For example, for the case shown in Fig. 13, sulfide formation occurs at 16% crystallization and the viscosity would be about 3 times the pure liquid viscosity (Vona et al., 2011), which would erase the gain in settling distance shown in Fig. 13b. Furthermore, at 28% or more crystals in the melt, the magma (a mixture of melt and crystals) has a viscosity more than 20 times the pure liquid viscosity and becomes non-Newtonian (Vona et al., 2011), meaning that the sulfide would settle less than without crystal formation. On the other hand, one may argue that magmatic sulfide ore formation requires slow cooling, which means that crystals will have time to settle. Hence, (1) whether the calculated effect is real or not cannot be assessed because the viscosity variation with melt composition is not well accounted for due to diverging trends of different models and because diffusivity variation with melt composition is not known, and (2) how effectively the crystals settle will have a major effect on the calculation. Nonetheless, the examples show that the effect of crystal fractionation, and by inference, magma assimilation and mixing, may potentially be large, although currently it cannot be evaluated accurately.

5. Discussion

5.1. Partitioning of ore elements

Segregation of a sulfide layer is only one of the critical steps in magmatic sulfide ore formation. The sulfide liquid must also collect ore elements such as Ni, Cu, and PGE to be a sulfide ore. Ore elements can be scavenged into sulfide liquid in at least two ways: one is by mass transfer during convective droplet growth and settling, and the second is by extraction from surrounding minerals such as olivine when the sulfide melt layer settles to the bottom of the magma chamber forming a mineral-sulfide melt mush. The former will be discussed in this subsection, and the latter will be discussed in the next subsection.

Chalcophile and siderophile elements partition strongly into sulfide melt during silicate-sulfide two-liquid equilibrium. The equilibrium partitioning has been discussed by Shaw (1970). Assume batch equilibrium in a closed system. Let $C_{i,0}$ be the initial concentration of element i in the silicate (or the bulk concentration in the system), $C_{i,sul}$ and $C_{i,sil}$ be the concentration (fraction or percent or ppm by mass) in the sulfide and silicate melts, K_i be the partition coefficient of i between sulfide and silicate melt, and F_{sul} and F_{sil} be the mass fraction of sulfide and silicate with $F_{sul} + F_{sil} = 1$, then the equilibrium condition is:

$$C_{i,sul}/C_{i,sil} = K_i, \tag{14}$$

and the mass balance condition is:

$$C_{i,sul}F_{sul} + C_{i,sil}F_{sil} = C_{i,0}. \tag{15}$$

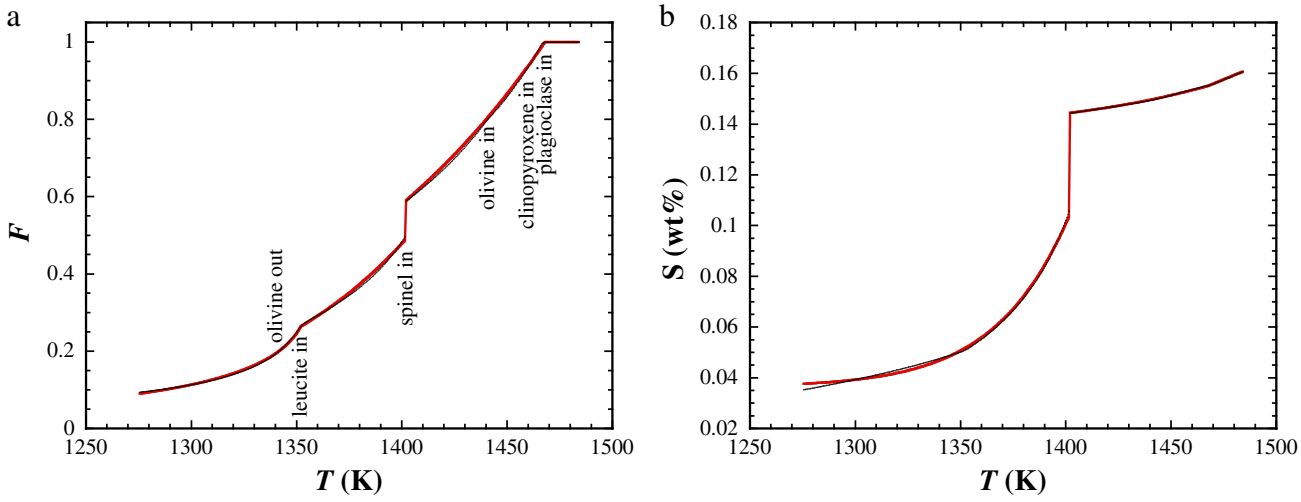

Fig. 12. (a) Calculated melt fraction as a function of temperature using the MELTS program (Ghiorso and Sack, 1995; Asimow and Ghiorso, 1998). The temperatures at which the major phases crystallize are also shown; (b) calculated S solubility of the fractionated melt using Li and Ripley (2009). The black dots are the calculated results and the red curve in each figure is a piecewise fit to the points. The sudden variation at 1399 K requires special handling. (For interpretation of the references to color in this figure legend, the reader is referred to the web version of this article.)

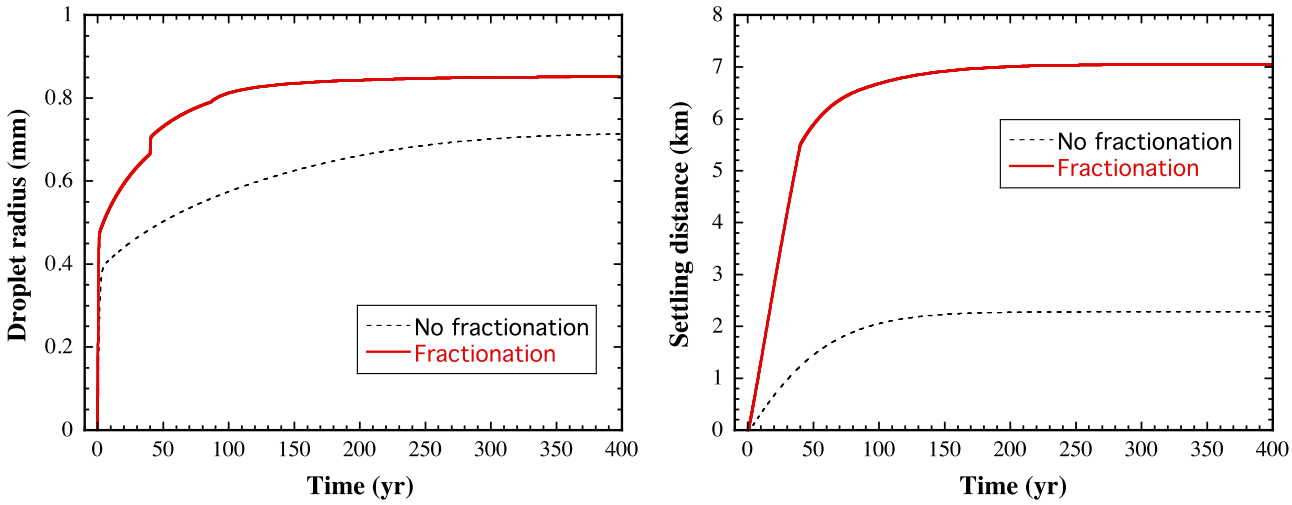

Fig. 13. Comparison of results without versus with consideration of crystal fractionation when the initial sulfur concentration is relatively low and when crystals settle rapidly.

Combining the above two equations leads to,

$$\frac{C_{i,\mathrm{sul}}}{C_{i,0}} = \frac{K_i}{F_{\mathrm{sil}} + K_i(1-F_{\mathrm{sil}})}. \tag{16}$$

To highlight the importance of the mass ratio of silicate to sulfide liquid ($F_{\mathrm{sil}}/F_{\mathrm{sul}}$), Campbell and Naldrett (1979) defined the R factor as: $R = F_{\mathrm{sil}} / F_{\mathrm{sul}}$ and expressed the above equation as

$$\frac{C_{i,\mathrm{sul}}}{C_{i,0}} = \frac{K_i(R+1)}{R+K_i}. \tag{17}$$

Understanding equilibrium partitioning is obviously important, but as shown in this work, for sulfide drop formation and settling, bulk equilibrium between sulfide melt and silicate melt is not always reached (interface equilibrium between the sulfide melt and silicate melt is assumed). Hence, the kinetics of the partitioning must also be considered. For example, there will be diffusive fractionation: ore elements with very high diffusivity in basaltic melts may be able to attain equilibrium distribution between sulfide drops and basaltic melts, but those with low diffusivity would deviate more from equilibrium partitioning. Mungall (2002a) discussed the kinetic controls on the partitioning of elements between silicate melt and a sulfide liquid drop, mostly for a liquid drop of a fixed size. Because sulfide drop growth and ore element partitioning occur simultaneously, it is necessary to consider kinetic control of elemental partitioning during sulfide drop growth. When the growth of a sinking sulfide drop was treated by Mungall (2002a), he used an old approach (Marsh, 1982). Here, we expand the approach in Section 2. Using the compositional boundary layer thickness concept, the mass transfer equation for an element i can be written as:

$$\frac{\mathrm{d}}{\mathrm{d}t}\left[\frac{4}{3}\pi a^3 \rho_{\mathrm{sul}} C_{i,0}(K_i - 1)\right] = 4\pi a^2 \rho_{\mathrm{sil}} D_i \frac{C_{i,\infty} - C_{i,0}}{\delta_i} \tag{18}$$

where subscript i means the element i, and D_i is the diffusivity of i in the silicate melt, and $C_{i,0}$ and $C_{i,\infty}$ are the concentrations of i in the interface and far-field silicate melt, respectively. Note that δ_i (the compositional boundary layer thickness for element i) may differ from δ (the compositional boundary layer thickness for sulfur) because the compositional boundary layer thickness depends on diffusivity (Eq. (7) in which Pe depends on D). The compositional boundary layer thickness with respect to element i can be found from $\delta_i = 2a / [1 + (1 + \mathrm{Pe}_i)^{1/3}] = 2a / [1 + (1 + 2aU / D_i)^{1/3}]$ (Kerr, 1995). In Eq. (18), δ_i, δ, a, C_∞, $C_{i,\infty}$, C_0, and $C_{i,0}$ all vary with time in a cooling magma chamber. Hence $C_{i,0}$ must be solved numerically. By letting $M = (4/3)\pi a^3 \rho_{\mathrm{sul}} C_{i,0}(K_i - 1)$, the left-hand side of Eq. (18) becomes $\mathrm{d}M/\mathrm{d}t$. Hence, once the right-hand of Eq. (18) is calculated using values from time step j, new M at time step $j + 1$ can be obtained, then new $C_{i,0}$ can be solved knowing M, then new $C_{i,\mathrm{sul}}$ can be calculated as $K_i C_{i,0}$, and the iteration continues.

In numerical simulations using the above procedures, the initial critical sulfide droplet is assumed to be in equilibrium with the silicate melt (accounting for the surface effect). Two sets of simulations were carried out: one assuming that $K_i = K_S$ (where K_S is the "partition coefficient" of sulfur, and it equals $C_{S,\mathrm{sul}}/C_{S,\mathrm{sil}}$ at equilibrium in which $C_{S,\mathrm{sul}}$ is a constant but $C_{S,\mathrm{sil}}$ depends on temperature), depending on temperature, and the other assuming temperature-independent K_i (Li and Audetat, 2012). The D_i/D_S ratio (where the subscript S means sulfur), x, N, and τ are varied parametrically. The simulation results are presented as θ_i versus time, where θ is the ratio of the apparent partition coefficient (concentration in the sulfide divided by concentration in the far-field silicate melt) to the equilibrium partition coefficient. Because the interface melts are assumed to be at equilibrium, θ is also the ratio of the concentration in the interface silicate melt to that in the far-field silicate melt ($\theta = K_{\mathrm{app}} / K_{\mathrm{eq}} = (C_{i,\mathrm{sul}}/C_{i,\infty}) / (C_{i,\mathrm{sul}}/C_{i,0}) = C_{i,0}/C_{i,\infty}$). When $\theta = 1$, it means the sulfide drop is in bulk equilibrium with the silicate melt. When $\theta = 0$, it means no ore element had time to diffuse into the sulfide drop. The assumption of equilibrium between the initial critical sulfide drop nucleus and the silicate melt means that $\theta = 1$ initially (in actuality, $\theta = 0.999$ to avoid numerical difficulties). A general result is that as the D_i/D_S ratio decreases, the final θ_i value (≤ 1) decreases as well, as expected.

When $K_i = K_S$ depending on temperature, the simulation results are shown in Fig. 14a–c for various values of x, N, and τ. Here the partition coefficient varies with time as the magma cools down. On the other hand, droplet growth only occurs in the early stage (e.g., typically when $t < \tau/2$), meaning that continued departure from equilibrium after growth ends is not meaningful. Hence, a vertical dashed line is shown when droplet reaches 99% of its final radius. The value of D_i/D_S plays a main role in controlling the departure from equilibrium, and varying other parameters does not change the behavior significantly. When the sulfide drop reaches 99% of its final radius, the partitioning of i is more than 96% in equilibrium when $D_i/D_S = 100$, about 92% when $D_i/D_S = 10$, 70–82% when $D_i/D_S = 1$, about 55% when $D_i/D_S = 0.1$, about 32–42% when $D_i/D_S = 0.01$, and about 19–28% when $D_i/D_S = 0.001$. That is, for elements with diffusivity larger than that of sulfur, the partitioning is not much (no more than 30%) different from equilibrium partitioning. On the other hand, for elements with diffusivities much smaller than that of sulfur, the kinetic departure from equilibrium can be as much as a factor 5.

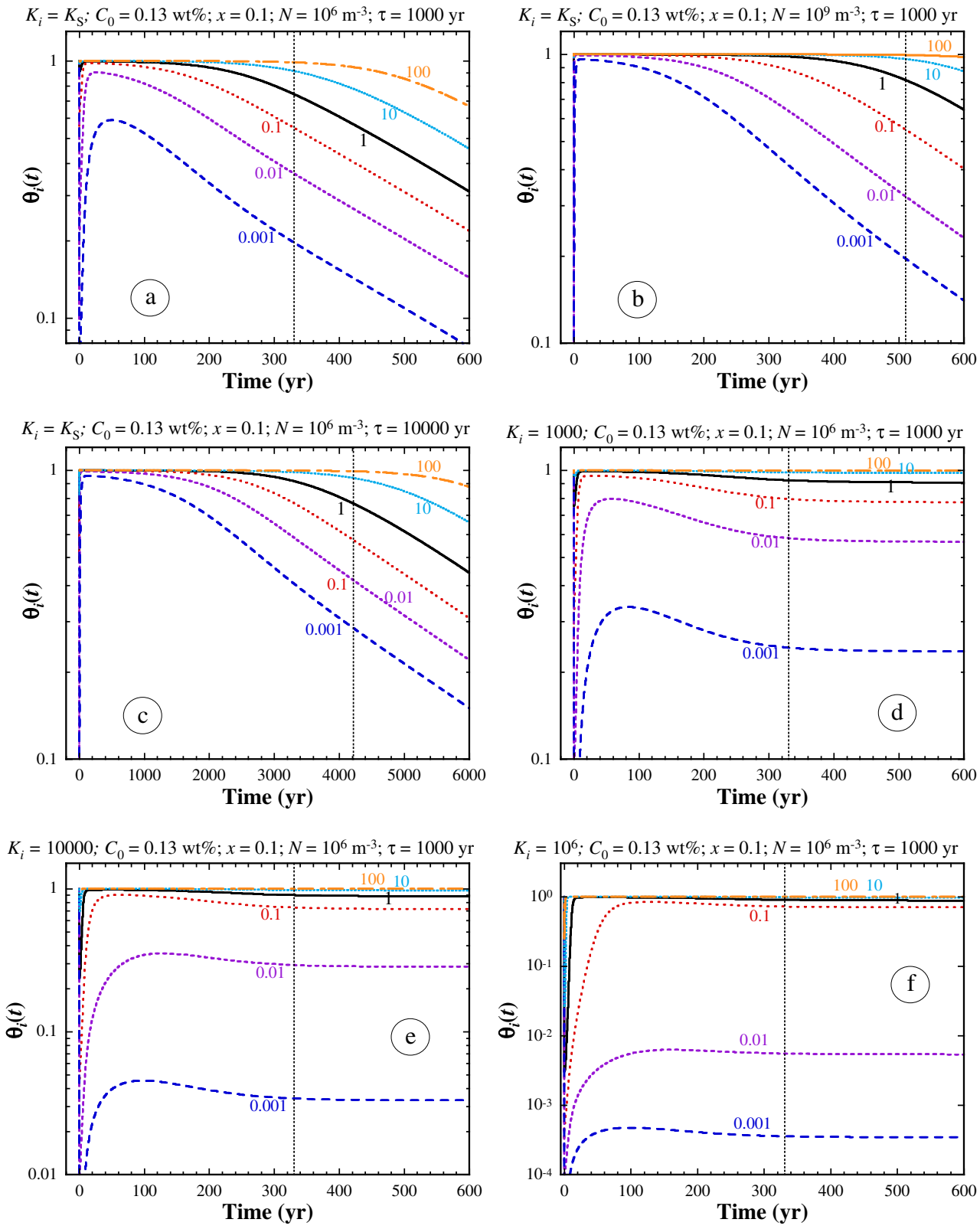

Fig. 14. Calculated results for the effectiveness of a freely falling sulfide drop to collect ore elements. The value on each curve indicates the D_i/D_S ratio. At $t = 0$, it is assumed that for the critical nucleus $\theta_i = 0.999$ (essentially at equilibrium). Often there is a rapid initial decrease in θ attributed to rapid initial growth due to high degree of oversaturation, but the amount of this initial growth is small. The vertical dashed line indicates the time when the droplet radius is 99% grown. Other parameters are given in each figure.

When K_i is independent of temperature, the simulation results are shown in Fig. 14d–f. For each specific case, because K_i does not vary, the departure from equilibrium gradually reaches a constant value, as expected because as time is increased, temperature is lowered, and the kinetics slows down. It can be seen that when $D_i/D_S \geq 1$, equilibrium partitioning is often ≥90% reached. On the other hand, when $D_i/D_S < 1$, the apparent equilibrium partition coefficient can be very different from the true K_i. Both K_i and D_i/D_S play a significant role in controlling how

close the equilibrium partitioning is reached. For example, when $D_i/D_S = 0.001$, $N = 10^6$ m^{-3}, $x = 0.1$, $C_0 = 0.13$ wt.%, and $\tau = 1000$ yr, the apparent partition coefficient (equaling $\theta_i K_i$) is 59, 236, 331, 344, and 346 for $K_i = 100$, 10^3, 10^4, 10^5, and 10^6, respectively. That is, when K_i is much larger than the "partition coefficient" for S and when $D_i/D_S \ll 1$, diffusive fractionation becomes very important. If the results are expressed as the ratio of concentration of element i in the sulfide over that in the equilibrium sulfide, the difference is smaller because C_i in sulfide does not depend strongly on K_i when K_i is large (Eq. (16)) but depends fairly strongly on the initial sulfur content through F_{sul}. These simulation results are different from the simple results in Mungall (2002a) because here sulfide drop growth and ore element transport in a finite silicate melt volume during cooling are all considered, whereas Mungall (2002a) mostly considered the diffusion of ore elements at a constant temperature into a sulfide drop of constant radius.

To apply the results to ore elements, it is necessary to know their partition coefficients between sulfide and basaltic melts and diffusivities in basaltic melts as a function of temperature. There is a large literature on the partition coefficients of these elements, and a slew of recent papers have advanced our knowledge of partition coefficients in a major way (Li and Audetat, 2012; Kiseeva and Wood, 2013; Patten et al., 2013; Mungall and Brenan, 2014). The partition coefficients decreases with increasing FeO content in the silicate melt in a relatively simple fashion (Kiseeva and Wood, 2013), and the temperature dependence is weak (Li and Audetat, 2012; Kiseeva and Wood, 2013). The values of the partition coefficients are 100–2130 for Cu (Li and Audetat, 2012; Kiseeva and Wood, 2013; Patten et al., 2013; Mungall and Brenan, 2014), 210–1400 for Ni (Li and Audetat, 2012; Kiseeva and Wood, 2013; Patten et al., 2013), 790 to 11,200 for Au (Li and Audetat, 2012; Mungall and Brenan, 2014), and of the order 10^5 to 10^6 for PGE (Mungall and Brenan, 2014). The diffusivity for many ore elements such as Cu, Au, Ni and PGE in basaltic melts has not been experimentally determined (Zhang et al., 2010). Using the model of Mungall (2002b) as a rough estimation for ore element diffusivities, in the temperature range of 1200–1500 K, the diffusivities of Cu^+, Au^+, Ni^{2+}, Fe^{2+}, Pt^{2+}, Rh^{2+}, Pd^{2+}, Ir^{2+}, Os^{3+}, and Ru^{3+} (valences and radii of these ions are from Mungall, 2002a to be consistent with the model of Mungall, 2002b) are respectively 23–310, 0.44–2.3, 0.14–1.4, 0.17–1.6, 0.18–1.6, 0.17–1.6, 0.20–1.7, 0.18–1.6, 0.004–0.2, and 0.004–0.2 times S diffusivity. Cu (high diffusivity) enrichment in sulfide melt would roughly follow bulk equilibrium partitioning, Au–Ni–Pt–Rh–Pd–Ir just slightly below equilibrium partitioning, but Os and Ru in sulfide melt are expected to be far lower than the equilibrium concentration. Note that the model of Mungall (2002b) could be orders of magnitude off (Behrens and Hahn, 2009; Zhang et al., 2010), and hence there is a need to experimentally determine diffusivities of the ore elements, especially those with smaller diffusivities than sulfur.

5.2. Extraction of Ni from olivine

There has been discussion about the need to avoid early olivine fractionation because olivine would sequester Ni from the magma, leaving low Ni concentration in later-formed sulfide melt (e.g., Simon and Ripley, 2011; Ripley and Li, 2013). Ripley and Li (2013) proposed a couple of mechanisms that may lead to sulfide liquid segregation before olivine crystallization, such as magma mixing and assimilation of country rocks. One additional way to suppress early olivine crystallization is by increasing magma chamber depth. For example, for the Etna basalt, calculations using MELTS (Ghiorso and Sack, 1995; Asimow and Ghiorso, 1998) show that at 200 MPa, olivine is the third phase to crystallize at 1440 K after 20% crystallization. However, at 500 MPa, olivine is the sixth phase to crystallize at 1418 K after 58% solidification. Many magmatic sulfide deposits are associated with MgO-rich melts in which olivine crystallizes earlier in the crystallization sequence but increasing magma chamber depth would still suppress olivine crystallization.

Even if olivine crystallizes early and takes away Ni from the magma, that does not prevent magmatic nickel sulfide ore formation. Here, I consider the interaction between olivine and sulfide melt when they both reach the bottom of a magma chamber and coexist in mush layer in which olivine crystals are immersed in sulfide melt, which is often observed (e.g., Chai and Naldrett, 1992). The extent to which Ni reequilibrates between olivine and sulfide melt is controlled by Ni diffusion in olivine. Petry et al. (2004) reported Ni diffusivity in olivine (Petry et al., 2004). At a temperature of 1373 K (moderately low temperature for a basaltic magma chamber), Ni diffusivity in olivine along c-axis is 5.2×10^{-17} m^2/s at QFM, meaning that an olivine crystal of 2.9 mm diameter would reach half equilibrium with the melt (meaning that half of the extra Ni mass in olivine would be extracted by the sulfide melt) in just 100 yr. That is, even if olivine crystallized and settled early, as long as sulfide melt settles and surrounds olivine, Ni can often be extracted from olivine to the sulfide melt. Therefore, for magmatic nickel sulfide ore formation, sulfide saturation does not have to be prior to olivine crystallization.

5.3. Formation of magmatic sulfide deposits in conduit systems?

Some authors have pointed out that sulfide deposits often form in features interpreted to be magmatic conduit systems (Chai and Naldrett, 1992; Li et al., 2000; Maier et al., 2001; Ding et al., 2010), meaning that sulfide-drop-rich magmas from a staging magma chamber intrude into a shallow magma chamber, and the sulfide drops settle at the opening of the magma ascent conduit, forming sulfide deposits. In the conduit-system scenario, this work would apply to the growth of sulfide drops in the deep-seated staging magma chamber before intrusion into the upper shallow-seated magma chamber.

Although the conduit model provides a reasonable explanation, alternative explanations of gravitational settling as explored here are also possible. For example, the occurrences of sulfide deposits in the conduit of a magmatic system can also be explained by sulfide drop settling and the subsequent gravitational flow of a sulfide melt layer (with olivine and other crystals floating in the melt) to the lowest regions of the magma chamber. For example, in the Jinchuan Ni–Cu–PGE sulfide deposit, the ore bodies occur not only in conduit-like structures, but also at the lower part of the intrusion (Li and Ripley, 2011), supporting a common mechanism for the formation of the deposit by fractionation, settling, and flow.

The conduit model is not without difficulties. One is that the presence of sulfide melt (and often high abundance of mafic minerals) would increase the overall density of the magma, making it less likely to ascend into a shallower magma chamber. Secondly, sometimes the crystal content is so high that a silicate melt containing such high abundance of crystals would not be able to flow at all. For example, Li and Ripley (2011) argued that for the western part of the Jinchuan sulfide deposit, due to the high proportion of olivine, a simple conduit injection model would not be feasible, and the original magma body must be much larger than what is now exposed. With a larger magma body, magma fractionation as modeled in this work becomes a viable contender for the formation of the sulfide deposit.

For the Jinchuan sulfide deposit, the massive and net-textured ores are often near the bottom of the Jinchuan intrusion and the disseminated ores lie above (Jia, 1986; Chai and Naldrett, 1992). This is consistent with gravitational settling in which sulfide drops that formed earlier and in the lower part of the intrusion would have time to settle to the bottom to form massive or net-textured ores, and the drops that formed later and in the upper part of the intrusion only settled to the disseminated zone. Chen et al. (2013) showed that the massive and the net-textured ores have higher PGE concentrations (e.g., 240–820 ppb Ir in the sulfide) in general than the disseminated ores (e.g., 120–560 ppb Ir in the sulfide), which supports the above interpretation: the earlier generation of sulfide drops that formed the massive or net-textured ores would have collected PGE from the original melt containing higher

PGE concentrations, and the later-formed sulfide drops that formed the disseminated ores could only collect the remaining PGE, leading to lower concentrations. The observed scatter and overlap in the PGE concentrations in different layers of ores would be consistent with a more general model in which droplets are allowed to nucleate continuously, because some sulfide in the disseminated zone would be from later-nucleated drops with lower PGE concentrations and some would be from drops that nucleated early in the upper part of the intrusion with higher PGE concentrations.

5.4. Further work

The ultimate goal of the model presented in this work is to evaluate ore potential of a magmatic body. For a given magmatic body, based on the mapped size, settling distance can be estimated and the cooling time scale can be evaluated. From the measured major oxide composition of the parental magma, melt viscosity, sulfur solubility and diffusivity as a function of temperature can be obtained from experimental data and models (more sulfur diffusion data are necessary). By studying melt inclusions in olivine and other minerals, it may be possible to estimate the initial sulfur concentration. It is also necessary to include crystal fractionation, assimilation, and magma mixing scenarios in the modeling of specific sulfide deposits although improvement of the general viscosity model and systematic study of S diffusion data are necessary to allow this.

Once these parameters are known, the growth kinetics and settling dynamics can be roughly modeled using this work to evaluate whether sulfide deposits can form. The remaining uncertainty is related to nucleation, which is deemed the most major uncertainty in this model. It is hoped that accurate homogeneous and heterogeneous nucleation theory will be developed, which would allow accurate calculation of nucleation rate as a function of temperature and the degree of oversaturation. Lacking such an accurate model, the two parameters for nucleation (x and N) used in this model may be empirically constrained by future studies of magmatic bodies both containing and lacking sulfide deposits.

The ability of the sulfide liquid to scavenge Ni–Cu–PGE depends on the initial concentrations and the diffusivity of the elements. It is hence necessary to remedy the lack of diffusivities for ore-forming elements.

Furthermore, the sulfide layer must survive later processes. Due to the low viscosity and high density of the sulfide melt, the sulfide melt pond at the bottom of a magma chamber has the tendency to undergo porous flow to the local low regions (such as conduit openings), and may even sink through a conduit into a deep-seated magma chamber. The sulfide melt may also intrude the country rocks or be lost into fault zones or due to later alteration.

6. Conclusions

A preliminary quantitative model is developed to evaluate the potential of a magmatic body to segregate sulfide melt layers and the ability of the sulfide melt to collect the ore elements. This model is a first step toward a fully quantitative and predictive model. Two major oversimplifications of the model need to be improved in the future: one is to quantify the nucleation rate, and the other is to fully incorporate crystal fractionation, assimilation and magma mixing. Improvement on the latter is possible with fractionation/assimilation/mixing models except for the lack of S diffusion data. Handling the nucleation rate may be improved empirically by studying magmatic bodies that are associated with versus those free of sulfide ores. It is also necessary to obtain experimental diffusivity data of S and other ore elements in various melts. Despite the oversimplifications and approximations, the preliminary model using real magma properties shows that magmatic sulfide deposits can form given an initial sulfur concentration that is typical in basaltic melt, 0.1 to 0.3 wt.%. Hence, the model may be applicable to common mafic melts. The critical parameters are the initial sulfur concentration and the cooling time scale of the magma, in addition to the less well-constrained nucleation parameters. Crystal fractionation tends to help the formation of sulfide deposits if the crystals settle, and would hinder the formation of sulfide deposits if the crystals stay in the magma. It is hoped that the model will contribute to a broader general understanding of the sulfide segregation process in magmas and will eventually be helpful to exploration geologists in finding sulfide ores.

Acknowledgment

I thank Ed Ripley for introducing me to the problems of magmatic sulfide deposits. Insightful and constructive comments by J.M. Brenan, Laurie Reisberg, Chusi Li, Ed Ripley, Adam Simon, Yuping Yang, Peng Ni and Yi Yu are highly appreciated. This work is partially supported by the US NSF (EAR-1019440).

References

Asimow, P.D., Ghiorso, M.S., 1998. Algorithmic modifications extending MELTS to calculate subsolidus phase relations. Am. Mineral. 83, 1127–1132.
Baker, D.R., Moretti, R., 2011. Modeling the solubility of sulfur in magmas: a 50-year old geochemical challenge. Rev. Mineral. Geochem. 73, 167–213.
Baker, L.L., Rutherford, M.J., 1996. Sulfur diffusion in rhyolite melts. Contrib. Mineral. Petrol. 123, 335–344.
Behrens, H., Hahn, M., 2009. Trace element diffusion and viscous flow in potassium-rich trachytic and phonolitic melts. Chem. Geol. 259, 63–77.
Behrens, H., Stelling, J., 2011. Diffusion and redox reactions of sulfur in silicate melts. Rev. Mineral. Geochem. 73, 79–111.
Bindeman, I.N., 2003. Crystal sizes in evolving silicic magma chambers. Geology 31, 367–370.
Bottinga, Y., Weill, D.F., 1972. The viscosity of magmatic silicate liquids: a model for calculation. Am. J. Sci. 272, 438–475.
Boudreau, A.E., Meurer, W.P., 1999. Chromatographic separation of the platinum-group elements, gold, base metals and sulfur during degassing of a compacting and solidifying igneous crystal pile. Contrib. Mineral. Petrol. 134, 174–185.
Bremond d'Ars, J.D.B., Arndt, N.T., Hallot, E., 2001. Analog experimental insights into the formation of magmatic sulfide deposits. Earth Planet. Sci. Lett. 186, 371–381.
Brenan, J.M., Haider, N., 2008. Experimental evaluation of liquid immiscibility in a portion of the system Fe–Ni–Cu–S using high gravitational acceleration. Econ. Geol. 103, 1563–1570.
Buchnan, D.L., Nolan, J., 1979. Solubility of sulfur and sulfide immiscibility in synthetic tholeiitic melts and their relevance to Bushveld-Complex rocks. Can. Mineral. 17, 483–494.
Campbell, I.H., Naldrett, A.J., 1979. The influence of silicate:sulfide ratios on the geochemistry of magmatic sulfides. Econ. Geol. 74, 1503–1505.
Carroll, M.R., Rutherford, M.J., 1987. The stability of igneous anhydrite: experimental results and implications for sulfur behavior in the 1982 El Chichon trachyandesite and other evolved magmas. J. Petrol. 28, 781–801.
Cashman, K.V., 1991. Textural constraints on the kinetics of crystallization of igneous rocks. Rev. Mineral. 24, 259–314.
Cashman, K.V., Marsh, B.D., 1988. Crystal size distribution (CSD) in rocks and the kinetics and dynamics of crystallization, II: Makaopuhi lava lake. Contrib. Mineral. Petrol. 99, 292–305.
Chai, G., Naldrett, A., 1992. The Jinchuan ultramafic intrusion: cumulate of a high-Mg basaltic magma. J. Petrol. 33, 277–303.
Chen, Y., Zhang, Y., 2008. Olivine dissolution in basaltic melt. Geochim. Cosmochim. Acta 72, 4756–4777.
Chen, Y., Zhang, Y., 2009. Clinopyroxene dissolution in basaltic melt. Geochim. Cosmochim. Acta 73, 5730–5747.
Chen, L.M., et al., 2013. Segregation and fractionation of magmatic Ni–Cu–PGE sulfides in the western Jinchuan intrusion, Northwestern China: insights from platinum group element geochemistry. Econ. Geol. 108, 1793–1811.
Clift, R., Grace, J.R., Weber, M.E., 1978. Bubbles, Drops, and Particles. Academic Press, New York, NY (380 pp.).
Deguen, R., Olson, P., Cardin, P., 2011. Experiments on turbulent metal-silicate mixing in a magma ocean. Earth Planet. Sci. Lett. 310, 303–313.
Ding, X., Li, C., Ripley, E.M., Rossell, D., Kamo, S., 2010. The Eagle and East Eagle sulfide ore-bearing mafic–ultramafic intrusions in the Midcontinent Rift System, upper Michigan: geochronology and petrologic evolution. Geochem. Geophys. Geosyst. 11, Q03003.
Fincham, C.J.B., Richardson, F.D., 1954. The behavior of sulfur in silicate and aluminate melts. Proc. R. Soc. Lond. A 223, 40–62.
Freda, C., Baker, D.R., Scarlato, P., 2005. Sulfur diffusion in basaltic melts. Geochim. Cosmochim. Acta 69, 5061–5069.
Gaetani, G.A., Grove, T.L., 1997. Partitioning of moderately siderophile elements among olivine, silicate melt, and sulfide melt: constraints on core formation in the Earth and Mars. Geochim. Cosmochim. Acta 61, 1829–1846.

Ghiorso, M.S., Sack, R.O., 1995. Chemical mass transfer in magmatic processes, IV: a revised and internally consistent thermodynamic model for the interpolation and extrapolation of liquid–solid equilibria in magmatic systems at elevated temperatures and pressures. Contrib. Mineral. Petrol. 119, 197–212.
Giordano, D., Dingwell, D.B., 2003. Viscosity of hydrous Etna basalt: implications for plinian-style basaltic eruptions. Bull. Volcanol. 65, 8–14.
Giordano, D., Russel, J.K., Dingwell, D., 2008. Viscosity of magmatic liquids: a model. Earth Planet. Sci. Lett. 271, 123–134.
Haughton, D.R., P.L., R., Skinner, B.J., 1974. Solubility of sulfur in mafic magmas. Econ. Geol. 69, 451–467.
Holzheid, A., 2010. Separation of sulfide melt droplets in sulfur saturated silicate liquids. Chem. Geol. 274, 127–135.
Holzheid, A., Grove, T.L., 2002. Sulfur saturation limits in silicate melts and their implications for core formation scenarios for terrestrial planets. Am. Mineral. 87, 227–237.
Hui, H., Zhang, Y., 2007. Toward a general viscosity equation for natural anhydrous and hydrous silicate melts. Geochim. Cosmochim. Acta 71, 403–416.
Hui, H., Zhang, Y., Xu, Z., Del Gaudio, P., Behrens, H., 2009. Pressure dependence of viscosity of rhyolitic melts. Geochim. Cosmochim. Acta 73, 3680–3693.
Ichikawa, H., Labrosse, S., Kurita, K., 2010. Direct numerical simulation of an iron rain in the magma ocean. J. Geophys. Res. 115, B01404. http://dx.doi.org/10.1029/2009JB0006427.
Jia, E.H., 1986. Geological characteristics of the Jinchuan Cu–Ni sulfide deposit in Gansu Province. Mineral Deposits 5, 27–38.
Jugo, P.J., 2009. Sulfur content at sulfide saturation in oxidized magmas. Geology 37, 415–418.
Jugo, P.J., Luth, R.W., Richards, J.P., 2005. An experimental study of the sulfur content in basaltic melts saturated with immiscible sulfide or sulfate liquids at 1300 °C and 1.0 GPa. J. Petrol. 46, 783–798.
Kerr, R.C., 1995. Convective crystal dissolution. Contrib. Mineral. Petrol. 121, 237–246.
Kiseeva, E.S., Wood, B.J., 2013. A simple model for chalcophile element partitioning between sulfide and silicate liquids with geochemical applications. Earth Planet. Sci. Lett. 383, 68–81.
Kress, V.C., Greene, L.E., Ortiz, M.D., Mioduszewski, L., 2008. Thermochemistry of sulfide liquids IV: density measurements and the thermodynamics of O–S–Fe–Ni–Cu liquid at low to moderate pressures. Contrib. Mineral. Petrol. 156, 785–797.
Lange, R.A., Carmichael, I.S.E., 1990. Thermodynamic properties of silicate liquids with an emphasis on density, thermal expansion and compressibility. Rev. Mineral. 24, 25–64.
Lange, R.A., Navrotsky, A., 1992. Heat capacities of Fe_2O_3-bearing silicate liquids. Contrib. Mineral. Petrol. 110, 985–999.
Levich, V.G., 1962. Physicochemical hydrodynamics. Physical and Chemical Engineering Sciences. Prentice-Hall, Englewood Cliff, N.J. (700 pp.).
Li, Y., Audetat, A., 2012. Partitioning of V, Mn, Co, Ni, Cu, Zn, As, Mo, Ag, Sn, Sb, W, Au, Pb, and Bi between sulfide phases and hydrous basanite melt at upper mantle conditions. Earth Planet. Sci. Lett. 355–356, 327–340.
Li, C., Ripley, E.M., 2005. Empirical equations to predict the sulfur content of mafic magmas at sulfide saturation and applications to magmatic sulfide deposits. Miner. Deposita 40, 218–230.
Li, C., Ripley, E.M., 2009. Sulfur contents at sulfide-liquid or anhydrite saturation in silicate melts: empirical equations and example applications. Econ. Geol. 104, 405–412.
Li, C., Ripley, E.M., 2011. The giant Jinchuan Ni–Cu–(PGE) deposit: tectonic setting, magma evolution, ore genesis, and exploration implications. Rev. Econ. Geol. 17, 163–180.
Li, C.S., Lightfoot, P.C., Amelin, Y., Naldrett, A.J., 2000. Contrasting petrological and geochemical relationships in the Voisey's Bay and Mushuau intrusions, Labrador, Canada: implications for ore genesis. Econ. Geol. 2000, 771–799.
Liu, Y., Samaha, N.T., Baker, D.R., 2007. Sulfur concentration at sulfide saturation (SCSS) in magmatic silicate melts. Geochim. Cosmochim. Acta 71, 1783–1799.
Luhr, J.F., 1990. Experimental phase relations of water- and sulfur-saturated arc magmas and the 1982 eruptions of El Chichon volcano. J. Petrol. 31, 1071–1114.
Maier, W.D., Li, C., Waal, S.A., 2001. Why are there no major Ni–Cu sulfide deposits in large layered mafic–ultramafic intrusions? Can. Mineral. 39, 547–556.
Marsh, B.D., 1982. On the mechanics of igneous diapirism, stoping, and zone melting. Am. J. Sci. 282, 808–855.
Marsh, B.D., 1989. Magma chambers. Ann. Rev. Earth Planet. Sci. 17, 439–474.
Mavrogenes, J.A., O'Neill, H.S.C., 1999. The relative effects of pressure, temperature and oxygen fugacity on the solubility of sulfide in mafic magmas. Geochim. Cosmochim. Acta 63, 1173–1180.
Misiti, V., et al., 2009. Viscosity of high-K basalt from the 5th April 2003 Stromboli paroxysmal explosion. Chem. Geol. 260, 278–285.
Misiti, V., et al., 2011. A general viscosity model of Campi Flegrei (Italy) melts. Chem. Geol. 290, 50–59.
Moretti, R., Baker, D.R., 2008. Modeling the interplay of fO2 and fS2 along the FeS-silicate melt equilibrium. Chem. Geol. 256, 286–298.
Moretti, R., Ottonello, G., 2005. Solubility and speciation of sulfur in silicate melts: the Conjugated Toop–Samis–Flood–Grjotheim (CTSFG) model. Geochim. Cosmochim. Acta 69, 801–823.
Mungall, J.E., 2002a. Kinetic controls on the partitioning of trace elements between silicate and sulfide liquids. J. Petrol. 43, 749–768.
Mungall, J.E., 2002b. Empirical models relating viscosity and tracer diffusion in magmatic silicate melts. Geochim. Cosmochim. Acta 66, 125–143.
Mungall, J.E., Brenan, J.M., 2014. Partitioning of platinum-group elements and Au between sulfide liquid and basalt and the origins of mantle–crust fractionation of the chacophile elements. Geochim. Cosmochim. Acta 125, 265–289.
Mungall, J.E., Naldrett, A.J., 2008. Ore deposits of the platinum-group elements. Elem. 4, 253–258.
Mungall, J.E., Su, S.G., 2005. Interfacial tension between magmatic sulfide and silicate liquids: constraints on kinetics of sulfide liquation and sulfide migration through silicate rocks. Earth Planet. Sci. Lett. 234, 135–149.
Naldrett, A.J., 1969. A portion of system Fe–S–O between 900 and 1080 degrees C and its application to sulfide ore magmas. J. Petrol. 10, 171–201.
Naldrett, A.J., 1989. Magmatic Sulfide Deposits. Oxford Univ Press, New York (186 pp.).
Naldrett, A.J., 2004. Magmatic Sulfide Deposits: Geology, Geochemistry and Exploration. Springer, Berlin (727 pp.).
Ochs, F.A., Lange, R.A., 1997. The partial molar volume, thermal expansivity, and compressibility of H_2O in silicate melts: new measurements and an internally consistent model. Contrib. Mineral. Petrol. 129, 155–165.
O'Neill, H.S.C., Mavrogenes, J.A., 2002. The sulfide capacity and the sulfur content at sulfide saturation of silicate melts at 1400 °C and 1 bar. J. Petrol. 43, 1049–1087.
Patten, C., Barnes, S.-J., Mathez, E.A., Jenner, F.E., 2013. Partition coefficients of chalcophile elements between sulfide and silicate melts and the early crystallization history of sulfide liquid: LA-ICP-MS analysis of MORB sulfide droplets. Chem. Geol. 358, 170–188.
Peach, C.L., Mathez, E.A., 1993. Sulfide melt–silicate melt distribution coefficients for nickel and iron and implications for the distribution of other chalcophile elements. Geochim. Cosmochim. Acta 57, 3013–3021.
Peach, C.L., Mathez, E.A., Keays, R.R., 1990. Sulfide melt-silicate melt distribution coefficients for noble metals and other chalcophile elements as deduced from MORB: implications for partial melting. Geochim. Cosmochim. Acta 54, 3379–3389.
Peach, C.L., Mathez, E.A., Keays, R.R., Reeves, S.J., 1994. Experimentally determined sulfide melt–silicate melt partition coefficients for iridium and palladium. Chem. Geol. 117, 361–377.
Petry, C., Chakraborty, S., Palme, H., 2004. Experimental determination of Ni diffusion coefficients in olivine and their dependence on temperature, composition, oxygen fugacity, and crystallographic orientation. Geochim. Cosmochim. Acta 68, 4179–4188.
Proussevitch, A.A., Sahagian, D.L., 1998. Dynamics and energetics of bubble growth in magmas: analytical formulation and numerical modeling. J. Geophys. Res. 103, 18223–18251.
Richet, P., 1984. Viscosity and configurational entropy of silicate melts. Geochim. Cosmochim. Acta 48, 471–483.
Richet, P., Lejeune, A., Holtz, F., Roux, J., 1996. Water and the viscosity of andesitic melts. Chem. Geol. 128, 185–197.
Ripley, E.M., Li, C., 2013. Sulfide saturation in mafic magmas: is external sulfur required for magmatic Ni–Cu–(PGE) ore genesis? Econ. Geol. 108, 45–58.
Rubie, D.C., Melosh, H.J., Reid, J.E., Liebske, C., Righter, K., 2003. Mechanisms of metal–silicate equilibration in the terrestrial magma ocean. Earth Planet. Sci. Lett. 205, 239–255.
Rubie, D.C., et al., 2011. Heterogeneous accretion, composition and core–mantle differentiation of the Earth. Earth Planet. Sci. Lett. 301, 31–42.
Scaillet, B., MacDonald, R., 2006. Experimental and thermodynamic constraints on the sulfur yield of peralkaline and metaluminous silicic flood eruptions. J. Petrol. 47, 1413–1437.
Schulze, F., Behrens, H., Holtz, F., Roux, J., Johannes, W., 1996. The influence of H2O on the viscosity of a haplogranitic melt. Am. Mineral. 81, 1155–1165.
Shafer, N.E., Zare, R.N., 1991. Through a beer glass darkly. Phys. Today 44 (10), 48–52.
Shaw, D.M., 1970. Trace element fractionation during anatexis. Geochim. Cosmochim. Acta 34, 237–243.
Shaw, H.R., 1972. Viscosities of magmatic silicate liquids: an empirical method of prediction. Am. J. Sci. 272, 870–893.
Shima, H., Naldrett, A.J., 1975. Solubility of sulfur in an ultramafic melt and the relevance of the system Fe–S–O. Econ. Geol. 70, 960–967.
Simon, A.C., Ripley, E.M., 2011. The role of magmatic sulfur in the formation of ore deposits. Rev. Mineral. Geochem. 73, 513–578.
Simon, A.C., Candela, P.A., Piccoli, P.M., Mengason, M., Englander, L., 2008. The effect of crystal–melt partitioning on the budgets of Cu, Au and Ag. Am. Mineral. 93, 1437–1448.
Vona, A., Romano, C., Dingwell, D.B., Giordano, D., 2011. The rheology of crystal-bearing basaltic magmas from Stromboli and Etna. Geochim. Cosmochim. Acta 75, 3214–3236.
Walker, D., Kiefer, W.S., 1985. Xenolith digestion in large magma bodies. J. Geophys. Res. 90, C585–C590.
Wallace, P., Carmichael, I.S.E., 1992. Sulfur in basaltic magmas. Geochim. Cosmochim. Acta 56, 1863–1874.
Watson, E.B., 1994. Diffusion in volatile-bearing magmas. Rev. Mineral. 30, 371–411.
Whittingon, A.G., et al., 2009. The viscosity of hydrous dacitic liquids: implications for the rheology of evolving silicic magmas. Bull. Volcanol. 71, 185–199.
Whittington, A., Richet, P., Holtz, F., 2000. Water and the viscosity of depolymerized aluminosilicate melts. Geochim. Cosmochim. Acta 64, 3725–3736.
Winther, K.T., Watson, E.B., Korenowski, G.M., 1998. Magmatic sulfur compounds and sulfur diffusion in albite melt at 1 GPa and 1300–1500 °C. Am. Mineral. 83, 1141–1151.
Zhang, Y., 1994. Reaction kinetics, geospeedometry, and relaxation theory. Earth Planet. Sci. Lett. 122, 373–391.
Zhang, Y., 2005. Fate of rising CO_2 droplets in seawater. Environ. Sci. Technol. 39, 7719–7724.
Zhang, Y., 2008. Geochemical Kinetics. Princeton University Press, Princeton, NJ (656 pp.).
Zhang, Y., 2013. Kinetics and dynamics of mass-transfer-controlled mineral and bubble dissolution or growth: a review. Eur. J. Mineral. 25, 255–266.
Zhang, Y., Xu, Z., 2003. Kinetics of convective crystal dissolution and melting, with applications to methane hydrate dissolution and dissociation in seawater. Earth Planet. Sci. Lett. 213, 133–148.

Zhang, Y., Xu, Z., 2007. A long-duration experiment on hydrous species geospeedometer and hydrous melt viscosity. Geochim. Cosmochim. Acta 71, 5226–5232.
Zhang, Y., Xu, Z., 2008. "Fizzics" of bubble growth in beer and champagne. Elem. 4, 47–49.
Zhang, Y., Walker, D., Lesher, C.E., 1989. Diffusive crystal dissolution. Contrib. Mineral. Petrol. 102, 492–513.
Zhang, Y., Xu, Z., Liu, Y., 2003. Viscosity of hydrous rhyolitic melts inferred from kinetic experiments, and a new viscosity model. Am. Mineral. 88, 1741–1752.
Zhang, Y., Xu, Z., Zhu, M., Wang, H., 2007. Silicate melt properties and volcanic eruptions. Rev. Geophys. 45, RG4004. http://dx.doi.org/10.1029/2006RG000216.
Zhang, Y., Ni, H., Chen, Y., 2010. Diffusion data in silicate melts. Rev. Mineral. Geochem. 72, 311–408.
Ziethe, R., 2009. Settling of metal droplets in a terrestrial magma ocean: on the correction of the Stokes velocity. Planet. Space Sci. 57, 306–317.